NUMERICAL APPROXIMATIONS OF THE MUMFORD-SHAH FUNCTIONAL FOR UNIT VECTOR FIELDS

JONAS HAEHNLE

ABSTRACT. Two numerical approximation schemes for minimising the Mumford-Shah functional for unit vector fields are proposed, analysed, and compared. The first uses a projection strategy, the second a penalisation strategy to enforce the sphere constraint. Both schemes are then applied to the segmentation of colour images using the Chromaticity and Brightness colour model.

1. INTRODUCTION

For $\Omega \subset \mathbb{R}^d$, and γ, α, λ positive constants, we are interested in numerically minimising the following weak version of the Mumford-Shah energy functional:

$$(1.1) \qquad G(\mathbf{u}) := \frac{\gamma}{2} \int_\Omega |\nabla \mathbf{u}|^2 \mathrm{d}\mathbf{x} + \alpha \mathcal{H}^{d-1}(S_\mathbf{u}) + \frac{\lambda}{2} \int_\Omega |\mathbf{u} - \mathbf{g}|^2 \mathrm{d}\mathbf{x},$$

with $\mathbf{u}, \mathbf{g} \in GSBV(\Omega, \mathbb{R}^m)$, and $|\mathbf{u}|^2 = 1$ a.e. (see Section 2 for definitions). This is a prototype problem for studying interesting effects with applications in image processing (see e.g. [43, 44, 8, 10, 19, 50, 7]), and liquid crystal theory (see e.g. [39, 42, 21, 51, 1, 6, 16]).

We are sometimes going to refer to functional (1.1) as the "Mumford-Shah" functional. It is, in fact, a version (for sphere-valued functions) of a functional proposed by De Giorgi, Carriero, and Leaci in [27] (for scalar functions) as a weak formulation of the original functional proposed by Mumford and Shah in [43] for greyscale image segmentation,

$$(1.2) \qquad E(u, K) := \frac{\gamma}{2} \int_{\Omega \setminus K} |\nabla u|^2 \mathrm{d}\mathbf{x} + \alpha \mathcal{H}^{d-1}(K) + \frac{\lambda}{2} \int_\Omega (u - g)^2 \mathrm{d}\mathbf{x},$$

with $g \in L^2(\Omega)$, which is to be minimised for all closed sets $K \subset \Omega$, and functions $u \in H^1(\Omega \setminus K)$. It is shown in [27] that the two problems are essentially equivalent.

The goal of image segmentation is to partition images into meaningful regions, which is often done by finding the edges which bound these regions, and which are in our case identified with the set K. The first term in (1.2) ensures smoothness of u outside of K, the second one ensures that there are not too many edges, and the last term ensures that the segmented image u does not deviate too much from the original one g.

A more concrete motivation for studying functional (1.1), therefore is *colour image segmentation* in the *Chromaticity and Brightness (CB)* colour model, where the chromaticity (colour information) is represented by an $\mathbb{S}^{m-1}$-valued function (usually $m = 3$) on the image domain Ω. The brightness, represented by a function $b : \Omega \to [0, 1]$, can be separately treated just like a greyscale image. It has been proposed that this model is well-suited for colour image processing. Osher and Vese [44] studied p-harmonic flows to the sphere ($p \geq 1$, in particular $p \in \{1, 2\}$), and applied them to image chromaticity, for example; other sources include [19, 50, 7] and references therein.

The name *free discontinuity problems* was introduced by De Giorgi in [24] for variational problems like (1.2), which consist of minimising a functional with volume and surface terms, depending on a closed set K and a function u (usually smooth outside K). Other early sources include [26, 25]. Weak formulations like (1.1) allow to prove existence of solutions (see [27] for the scalar, and [17] for the sphere-valued case), but still require the computation of geometric properties of the unknown set of discontinuity boundaries.

Therefore, Ambrosio and Tortorelli introduced an elliptic approximation in [3, 4], whose vectorial version, if defined for sphere-valued functions, is to minimise

(1.3)
$$AT_\varepsilon(\mathbf{u}, s) := \frac{\gamma}{2} \int_\Omega \left(s^2 + k_\varepsilon \right) |\nabla \mathbf{u}|^2 \, \mathrm{d}\mathbf{x} + \alpha \int_\Omega \left(\varepsilon |\nabla s|^2 + \frac{1}{4\varepsilon}(1-s)^2 \right) \mathrm{d}\mathbf{x}$$
$$+ \frac{\lambda}{2} \int_\Omega |\mathbf{u} - \mathbf{g}|^2 \, \mathrm{d}\mathbf{x}$$

for $\mathbf{u}, \mathbf{g} \in H^1\left(\Omega, \mathbb{S}^{m-1}\right)$, $s \in H^1(\Omega, [0,1])$, $0 < \varepsilon, k_\varepsilon \ll 1$, and $k_\varepsilon = o(\varepsilon)$. Here, s is a *phase function* approximating $1 - \chi_K$ by penalisation of phase transitions. Ambrosio and Tortorelli showed Γ-convergence of $AT_\varepsilon(\mathbf{u}, s)$ to $G(\mathbf{u})$ in L^2 in the scalar ([3, 4]), as well as the $\mathbb{S}^{m-1}$-valued case ([4]) for $\varepsilon \to 0$.

Bellettini and Coscia carried out a finite element approximation of the Mumford-Shah functional in the scalar case, based on this elliptic approximation in [8]. They showed that their approximation $G_{\varepsilon,h} : V^h(\Omega) \times V^h(\Omega, [0,1]) \to \overline{\mathbb{R}}$ is Γ-convergent to $G : H^1(\Omega) \times H^1(\Omega) \to \overline{\mathbb{R}}$ provided that the mesh size fulfils $h = o(k_\varepsilon)$, and that S_u is piecewise C^2. Here, $V^h(\Omega)$ is the continuous, piecewise affine finite element space. Using the approximation result in [28], Bourdin in [10] showed that S_u does not need to be assumed piecewise C^2; and he proposed an algorithm for actual computations — without providing a proof for its convergence, though. The problem here is that the two variables u and s appear strongly coupled in the energy and in the corresponding gradient flow.

As an alternative to the above phase-field approximation of the Mumford-Shah functional, Braides and Dal Maso proposed a non-local approximation approach in [13], on which Cortesani based a Γ-convergent, vector-valued finite element approximation in [22].

A different motivation for (1.3) comes from the theory of *nematic liquid crystals.* In order to overcome mathematical difficulties in showing existence and regularity of energy minimising static configurations in the Oseen-Frank model, Lin in [39] adapts Ericksen's energy, which he simplifies to (see [39, equation (3.12)])

$$\int_\Omega \frac{1}{2} s^2 |\nabla \mathbf{n}|^2 + |\nabla s|^2 + W_0(s) \, \mathrm{d}\mathbf{x}$$

with variable degree of orientation $s \in [-1/2, 1]$ (in experiments, often $s \geq 0$), and director $\mathbf{n}$, $|\mathbf{n}| = 1$ a.e. The strong similarities of this energy to functional (1.3) lets us hope that our analysis may be of use to this application, too.

The overall goal of the present work is to construct and analyse convergent discretisations for a prototype problem with several non-convexities; namely, we consider a non-convex functional (the Mumford-Shah functional) with a non-convex constraint (the sphere constraint), as an extension to existing work on convex functionals (in particular harmonic maps) with non-convex constraints, which have been intensely studied (see e.g. [1, 5, 6] and references therein). In particular, we deal with discretisations of the sphere constraint, which we account for using a projection and a penalisation strategy. The former turns out to deliver more convincing computational results, while the latter is analytically more satisfactory.

Below, we give a short overview over the two methods for the approximation of (1.1) that we shall present in Sections 3 – 7 of this paper, where we in particular discuss relevant stability properties of computed approximations, such as

- energy decay property for splitting schemes related to (1.3),
- the validity of a discrete or penalised sphere constraint for approximations of $\mathbf{u}$, and
- non-negativity and upper bounds for approximations of the phase field function s.

1.1. **Splitting & Projection Strategy.** The problem of coupled variables is addressed through an iterative splitting strategy; i.e., in every step of the iteration the energy is first minimised with respect to the first variable while keeping the second variable fixed, and then minimised with respect to the second variable while keeping the first one fixed. A special projection idea as proposed by Alouges in [1] is used to enforce the sphere constraint. We propose a first-order finite element discretisation, which preserves the sphere constraint exactly at nodal points. The resulting discrete algorithm is simple, results in only linear equations to be solved in every step of the iteration, and every step is energy-decreasing (for acute triangulations). The algorithm converges weakly (up to subsequences) in $H^1 \times H^1$ to a tuple $(\mathbf{u}, s) \in H^1\left(\Omega, \mathbb{S}^{m-1}\right) \times H^1(\Omega)$. For $d = 2$ we can show that s and iterates S_n fulfil $S_n, s \in [-1, 1]$. However, we cannot show that $(\mathbf{u}, s)$ is a stationary point of the Ambrosio-Tortorelli energy for unit vector fields.

1.2. **Penalisation & Splitting Strategy.** This method again uses a splitting strategy, but the sphere constraint is now approximated by penalisation; i.e., we add a Ginzburg-Landau term $\frac{1}{4\delta_\varepsilon} \int_\Omega \left(|\mathbf{u}|^2 - 1\right)^2 \mathrm{d}\mathbf{x}$ $(0 < \delta \ll 1)$ to the energy (1.3). We show that for proper scales of δ_ε in terms of ε, this does not affect Γ-convergence. Furthermore, we propose a first-order finite element algorithm based on this splitting and penalisation strategy. The resulting algorithm converges weakly (up to subsequences) in $H^1 \times H^1$ to a tuple $(\mathbf{u}, s) \in H^1(\Omega, \mathbb{R}^m) \times H^1(\Omega)$, without any mesh-constraint. For $d = 2$ we can also show that $S_n, s \in [-1, 1]$. This allows to get strong convergence (up to subsequences) of iterates $\mathbf{U}_n$ in H^1, which in turn allows to pass to the limit and show that $(\mathbf{u}, s)$ is a stationary point of the Ambrosio-Tortorelli-Ginzburg-Landau energy, and that $s \geq 0$. However, we now have to solve a nonlinear equation in every iteration.

In Section 6, comparative computational experiments for the "Penalisation & Splitting" and the "Splitting & Projection" methods are presented, which address in particular

(1) the effect of perturbing the sphere constraint throughout minimisation, as well as proper scalings of regularisation and numerical parameters;
(2) the accuracy of zero sets of s in the course of minimisation; and
(3) comparative numerical studies to relate the CB and RGB models in colour image segmentation.

2. PRELIMINARIES

We often use c and C as generic non-negative constants, capital letters for finite element functions and boldface for vectors or vector-valued functions. Given $\mathbf{x}, \mathbf{y} \in \mathbb{R}^d$, $\langle \mathbf{x}, \mathbf{y} \rangle$ or $\mathbf{x} \cdot \mathbf{y}$ will denote their standard scalar product, and $|\mathbf{x}|$ the Euclidean norm of $\mathbf{x}$. For a set S, $|S|$ or $\mathcal{L}^d(S)$ denotes its Lebesgue measure of dimension d, $\mathcal{H}^d(S)$ its Hausdorff measure. The L^2 scalar product and norm will be denoted by $(\cdot, \cdot)$ and $\|\cdot\|$, respectively, and $\mathbb{S}^{m-1}$ will be the unit sphere in $\mathbb{R}^m$. For $a, b \in \mathbb{R}$, let $a \wedge b := \min\{a, b\}$, and $a \vee b := \max\{a, b\}$. By $A : B$ for $A, B \in \mathbb{R}^{m \times m}$ we denote the dyadic product; i.e., $A : B := \sum_{i,j=1}^m a_{ij} b_{ij}$ for $A = (a_{ij})$, $B = (b_{ij})$. Let $|A|$ denote the Frobenius norm of A; i.e., $|A|^2 := \sum_{i,j=1}^m |a_{ij}|^2$. For two vectors $\mathbf{a} \in \mathbb{R}^d$, $\mathbf{b} \in \mathbb{R}^m$, let $\mathbf{a} \otimes \mathbf{b} := M$ denote the matrix with entries $m_{ij} := \mathbf{a}_i \mathbf{b}_j$.

2.1. **Functions of Bounded Variation and Γ-Convergence.** We summarise some definitions and results on functions of bounded variation and Γ-convergence. Sources are e.g. [2, 35, 30, 23, 11, 12, 18].

2.1.1. *BV, SBV, and GSBV Functions.* Let $\Omega \subset \mathbb{R}^d$ be a bounded open set, $\mathbf{u} : \Omega \to \mathbb{R}^m$ a measurable function, $S := \mathbb{R}^m \cup \{\infty\}$, and $\mathbf{x} \in \Omega$ be fixed. We call $\mathbf{z} \in S$ the *approximate limit* of $\mathbf{u}$ at $\mathbf{x}$, or $\mathbf{z} = \mathrm{ap} - \lim_{\mathbf{y} \to \mathbf{x}} \mathbf{u}(\mathbf{y})$, if for every neighbourhood U of $\mathbf{z} \in S$ we have

$$\lim_{\varrho \to \infty} \frac{1}{\varrho^n} |\{\mathbf{y} \in \Omega : |\mathbf{y} - \mathbf{x}| < \varrho, \mathbf{u}(\mathbf{y}) \notin U\}| = 0.$$

If $\mathbf{z} \in \mathbb{R}^m$, we call $\mathbf{x}$ a *Lebesgue point* of $\mathbf{u}$, and we denote by $S_{\mathbf{u}}$ the complement of the set of Lebesgue points of $\mathbf{u}$ (*approximate discontinuity set*). Since $|S_{\mathbf{u}}|$ is known to be zero, $\mathbf{u} = \widetilde{\mathbf{u}}$ a.e. for

$$\widetilde{\mathbf{u}}(\mathbf{x}) := \mathrm{ap} - \lim_{\substack{\mathbf{y} \to \mathbf{x} \\ \mathbf{y} \in \Omega}} \mathbf{u}(\mathbf{y}).$$

Let $\mathbf{x} \in \Omega \setminus S_{\mathbf{u}}$ such that $\widetilde{\mathbf{u}}(\mathbf{x}) \neq \infty$. If there exists $L \in \mathbb{R}^{d \times m}$ such that

$$\mathrm{ap} - \lim_{\substack{\mathbf{y} \to \mathbf{x} \\ \mathbf{y} \in \Omega}} \frac{|\mathbf{u}(\mathbf{y}) - \widetilde{\mathbf{u}}(\mathbf{x}) - L(\mathbf{y} - \mathbf{x})|}{|\mathbf{y} - \mathbf{x}|} = 0,$$

we call $\mathbf{u}$ *approximately differentiable* in $\mathbf{x}$, and $\nabla \mathbf{u}(\mathbf{x}) := L$ the (uniquely determined) *approximate gradient* of $\mathbf{u}$ in $\mathbf{x}$. A function $\mathbf{u} \in L^1(\Omega, \mathbb{R}^m)$ is called a *function of bounded variation* in Ω, or $\mathbf{u} \in BV(\Omega, \mathbb{R}^m)$, if its distributional derivative $D\mathbf{u}$ is representable by a measure with finite total variation $|D\mathbf{u}|(\Omega)$; i.e., if

$$\sum_{\alpha=1}^m \int_\Omega u^\alpha \mathrm{div}\,(\varphi^\alpha)\,\mathrm{d}\mathbf{x} = -\sum_{\alpha=1}^m \sum_{i=1}^d \int_\Omega \varphi_i^\alpha \mathrm{d}D_i u^\alpha \qquad \forall \varphi \in C_c^1\left(\Omega, \mathbb{R}^{m \times d}\right),$$

with $D\mathbf{u}$ an $\mathbb{R}^{d \times m}$ valued matrix of measures $D_i u^\alpha$, and $\mathbf{u} = (u_1, \ldots, u_m)$. Defining

$$\|\mathbf{u}\|_{BV(\Omega, \mathbb{R}^m)} := \|\mathbf{u}\|_{L^1(\Omega, \mathbb{R}^m)} + |D\mathbf{u}|(\Omega),$$

makes $BV(\Omega, \mathbb{R}^m)$ a Banach space.

If $\{\mathbf{u}_j\} \subset BV(\Omega, \mathbb{R}^m)$ with $\sup_j \|\mathbf{u}_j\|_{BV(\Omega, \mathbb{R}^m)} < +\infty$, then there exist a subsequence $\{\mathbf{u}_{j_k}\}$ and a function $\mathbf{u} \in BV(\Omega, \mathbb{R}^m)$ such that $\mathbf{u}_{j_k} \to \mathbf{u}$ in $L^1(\Omega, \mathbb{R}^m)$, and $D\mathbf{u}_{j_k} \to D\mathbf{u}$ weakly-$*$ in the sense of measures.

Also, for $\mathbf{u} \in BV(\Omega, \mathbb{R}^m)$, $S_{\mathbf{u}}$ is countably $\mathcal{H}^{d-1}$-rectifiable; i.e.,

$$S_{\mathbf{u}} = N \cup \bigcup_{i \in \mathbb{N}} K_i,$$

where $\mathcal{H}^{d-1}(N) = 0$, and each K_i is a compact subset of a C^1 manifold. So, for $\mathcal{H}^{d-1}$-a.e. $\mathbf{y} \in S_{\mathbf{u}}$ we can define an *exterior unit normal* $\boldsymbol{\nu}_{\mathbf{u}}$ and *outer* and *inner traces* of $\mathbf{u}$ on $S_{\mathbf{u}}$ by

$$\mathbf{u}^{\pm}(\mathbf{x}) := \mathrm{ap} - \lim_{\substack{\mathbf{y} \to \mathbf{x} \\ \mathbf{y} \in \pi^{\pm}(\mathbf{x}, \boldsymbol{\nu}_{\mathbf{u}}(\mathbf{x}))}} \mathbf{u}(\mathbf{y}),$$

with $\pi^{\pm}(\mathbf{x}, \boldsymbol{\nu}_{\mathbf{u}}(\mathbf{x})) := \{\mathbf{y} \in \mathbb{R}^d : \pm\langle \mathbf{y} - \mathbf{x}, \boldsymbol{\nu}_{\mathbf{u}}(\mathbf{x})\rangle > 0\}$. A point $\mathbf{x} \in \Omega$ is called a *jump point* of $\mathbf{u}$, $\mathbf{x} \in J_{\mathbf{u}}$, if there exists $\boldsymbol{\nu} \in \mathbb{S}^{d-1}$, such that

$$\mathrm{ap} - \lim_{\substack{\mathbf{y} \to \mathbf{x} \\ \mathbf{y} \in \pi^-(\mathbf{x}, \boldsymbol{\nu})}} \mathbf{u}(\mathbf{y}) \neq \mathrm{ap} - \lim_{\substack{\mathbf{y} \to \mathbf{x} \\ \mathbf{y} \in \pi^+(\mathbf{x}, \boldsymbol{\nu})}} \mathbf{u}(\mathbf{y}).$$

It is known that $J_{\mathbf{u}} \subseteq S_{\mathbf{u}}$, and $\mathcal{H}^{d-1}(S_{\mathbf{u}} \setminus J_{\mathbf{u}}) = 0$.

If we decompose $D\mathbf{u}$ into an absolutely continuous part $D^a\mathbf{u}$ and a singular part $D^s\mathbf{u}$, both with respect to the Lebesgue measure $\mathcal{L}^d$, $D\mathbf{u} = D^a\mathbf{u} + D^s\mathbf{u}$, the density of $D^a\mathbf{u}$ with respect to $\mathcal{L}^d$ coincides with the approximate gradient $\nabla\mathbf{u}$ $\mathcal{L}^d$-a.e. The restriction $D^j\mathbf{u}$ of $D^s\mathbf{u}$ to $S_{\mathbf{u}}$ is called *jump part* of $D\mathbf{u}$, the restriction $D^c\mathbf{u}$ of $D^s\mathbf{u}$ to $\Omega \setminus S_{\mathbf{u}}$ it called *Cantor part*. So,

$$D\mathbf{u} = D^a\mathbf{u} + D^j\mathbf{u} + D^c\mathbf{u}.$$

It is known that $D^j\mathbf{u} = (\mathbf{u}^+ - \mathbf{u}^-) \otimes \boldsymbol{\nu}_{\mathbf{u}} \mathcal{H}^{d-1}\lfloor S_{\mathbf{u}}$.

A function $\mathbf{u} \in BV(\Omega, \mathbb{R}^m)$ is called a *special function of bounded variation* in Ω, $\mathbf{u} \in SBV(\Omega, \mathbb{R}^m)$, if $D^c\mathbf{u} = 0$. We call $\mathbf{u} \in BV(\Omega, \mathbb{R}^m)$ a *generalised special function of bounded variation*, $\mathbf{u} \in GSBV(\Omega, \mathbb{R}^m)$, if $\mathbf{g}(\mathbf{u}) \in SBV(\Omega, \mathbb{R}^m)$ for every $\mathbf{g} \in C^1(\mathbb{R}^m)$ such that $\nabla\mathbf{g}$ has compact support. For $1 < p < +\infty$, let

$$(G)SBV^p(\Omega, \mathbb{R}^m) := \left\{ \mathbf{u} \in (G)SBV(\Omega, \mathbb{R}^m) : \mathcal{H}^{d-1}(J_{\mathbf{u}}) < +\infty, \ \nabla\mathbf{u} \in L^p(\Omega, \mathbb{R}^{d \times m}) \right\}.$$

We remark that $W^{1,1}(\Omega, \mathbb{R}^m) \subsetneq BV(\Omega, \mathbb{R}^m)$, that $\mathbf{u} \in SBV(\Omega, R^m)$ implies $\mathbf{u} \in W^{1,1}(\Omega \setminus \overline{S_{\mathbf{u}}}, \mathbb{R}^m)$, and that $SBV(\Omega, \mathbb{R}^m) \cap L^\infty(\Omega, \mathbb{R}^m) = GSBV(\Omega, \mathbb{R}^m) \cap L^\infty(\Omega, \mathbb{R}^m)$.

2.1.2. Γ-*Convergence.* Let X be a separable Banach space with a topology τ and let $F_\varepsilon : X \to \overline{\mathbb{R}}$ be a sequence of functionals. We say F_ε Γ-*converges* to F in the topology τ, or $F = \Gamma - \lim_{\varepsilon \to 0} F_\varepsilon$, if the following two conditions hold:

(1) For every $x \in X$ and for every sequence $\{x_\varepsilon\} \subset X$ τ-converging to $x \in X$,

$$F(x) \leq \liminf_{\varepsilon \to 0} F_\varepsilon(x_\varepsilon),$$

(2) For every $x \in X$ there exists a sequence $\{x_\varepsilon\} \subset X$ (*recovery sequence*) τ-converging to $x \in X$, such that

$$F(x) \geq \limsup_{\varepsilon \to 0} F_\varepsilon(x_\varepsilon).$$

Lemma 2.1. *Let $F_\varepsilon, F : X \to \overline{\mathbb{R}}$, with $\Gamma - \lim_{\varepsilon \to 0} F_\varepsilon = F$. Then*

(1) *F is lower semicontinuous on X.*
(2) *$F + G = \Gamma - \lim (F_\varepsilon + G)$ for all continuous $G : X \to \mathbb{R}$.*
(3) *Let $\{\mathbf{u}_\varepsilon\} \subset X$ be such that*

$$\lim_{\varepsilon \to 0^+} \left(F_\varepsilon(\mathbf{u}_\varepsilon) - \inf_X F_\varepsilon \right) = 0,$$

then every cluster point $\mathbf{u}$ of $\{\mathbf{u}_\varepsilon\}$ minimises F over X, and

$$\lim_{\varepsilon \to 0^+} \inf_X F_\varepsilon = \min_X F = F(\mathbf{u}).$$

Here are some connections between Γ-convergence and pointwise convergence:

- If F_ε converges uniformly to F, then F_ε Γ-converges to F.
- If F_ε is decreasing and converges pointwise to F, then F_ε Γ-converges to RF, the lower semicontinuous envelope of F.

3. Splitting & Projection Algorithm

Let $\Omega \subset \mathbb{R}^d$ be a polyhedral Lipschitz domain, and $\mathcal{T}_h$ be a quasi-uniform triangulation of Ω with node set $\mathcal{N}$ and maximal mesh size $h > 0$ (c.f. [14]). The space of globally continuous, piecewise affine finite element functions on $\mathcal{T}_h$ is denoted by $V_h(\Omega) \subseteq H^1(\Omega)$. The nodal basis functions are $\{\varphi_{\mathbf{z}} : \mathbf{z} \in \mathcal{N}\} \subseteq V_h(\Omega)$. Let $V_h(\Omega, \mathbb{R}^m)$ be the finite element space of $\mathbb{R}^m$-valued mappings with basis functions $\{\boldsymbol{\varphi}_{\mathbf{z}}^i : \mathbf{z} \in \mathcal{N}, 1 \leq i \leq m\}$, with $\boldsymbol{\varphi}_{\mathbf{z}}^1 := (\varphi_{\mathbf{z}}, 0, \dots)^T \in V_h(\Omega, \mathbb{R}^m)$, $\boldsymbol{\varphi}_{\mathbf{z}}^2 := (0, \varphi_{\mathbf{z}}, 0, \dots)^T \in V_h(\Omega, \mathbb{R}^m)$, and so forth. Let $\mathcal{I}_h(\cdot) : C^0(\overline{\Omega}) \to V_h(\Omega)$ be the Lagrange interpolation operator, and $R_h(\cdot) : H^1(\Omega) \to V_h(\Omega)$ the Ritz projection, defined by

$$(\nabla(R_h(\varphi) - \varphi), \nabla V) + (R_h(\varphi) - \varphi, V) = 0 \quad \forall V \in V_h(\Omega),$$

and $r_h(\cdot) : L^2(\Omega) \to V_h(\Omega)$ the Clément operator [20] ($\mathcal{I}_h(\cdot)$, $\mathbf{R}_h(\cdot)$, and $\mathbf{r}_h(\cdot)$ in the vector valued case). The latter operator will be needed since it can be applied to non-continuous functions.

Lemma 3.1. *The tuple* $(\mathbf{u}, s) \in H^1(\Omega, \mathbb{S}^{m-1}) \times H^1(\Omega, [0, 1])$ *is a stationary point of* $AT_\varepsilon(\cdot, \cdot)$ *if and only if*

$$\gamma\left(\left(s^2 + k_\varepsilon\right) \nabla \mathbf{u}, \nabla \boldsymbol{\varphi}\right) = \lambda(\mathbf{g}, \boldsymbol{\varphi}) \tag{3.1}$$

for all $\boldsymbol{\varphi} \in H^1(\Omega, \mathbb{R}^m)$ *such that* $\boldsymbol{\varphi}(\mathbf{x}) \in T_{\mathbf{u}(\mathbf{x})}\mathbb{S}^{m-1}$ *(the tangent space of* $\mathbb{S}^{m-1}$ *at* $\mathbf{u}(\mathbf{x})$*), and*

$$2\alpha\varepsilon(\nabla s, \nabla \varphi) + \left(\left(\gamma|\nabla \mathbf{u}|^2 + \frac{\alpha}{2\varepsilon}\right) s, \varphi\right) = \left(\frac{\alpha}{2\varepsilon}, \varphi\right) \tag{3.2}$$

for all $\varphi \in H^1(\Omega) \cap L^\infty(\Omega)$.

Proof. Note $\mathbf{u} \cdot \boldsymbol{\varphi} = 0$ a.e. and derive the first variation of $AT_\varepsilon(\cdot, \cdot)$ with respect to $\mathbf{u}$ and s, respectively, c.f. [49] and [15, Proposition 1]. $\square$

The most natural approach to the discrete case would be to work with the original functional $AT_\varepsilon(\cdot, \cdot)$. However, it is not clear how to get a uniform L^∞ bound on iterates S_n in this setting. We therefore introduce mass lumping into the last term: For $\mathbf{G} \in V_h(\Omega, \mathbb{R}^m)$, we define

$$\begin{aligned} E_h(\mathbf{U}, S) \;:=\; & \frac{\gamma}{2} \int_\Omega \left(S^2 + k_\varepsilon\right) |\nabla \mathbf{U}|^2 \, d\mathbf{x} + \frac{\lambda}{2} \int_\Omega |\mathbf{U} - \mathbf{G}|^2 \, d\mathbf{x} \\ & + \alpha \int_\Omega \varepsilon |\nabla S|^2 + \frac{1}{4\varepsilon} \mathcal{I}_h\left((1-S)^2\right) d\mathbf{x}, \end{aligned}$$

and

$$\widetilde{E}(\mathbf{U}, S) := \frac{\gamma}{2} \int_\Omega \left(S^2 + k_\varepsilon\right) |\nabla \mathbf{U}|^2 \, d\mathbf{x} + \frac{\lambda}{2} \int_\Omega |\mathbf{U} - \mathbf{G}|^2 \, d\mathbf{x},$$

with $\gamma, \alpha, \varepsilon, k_\varepsilon$ fixed and positive, and $\lambda \geq 0$. We also assume $d \leq 2$, since so far, our arguments for the L^∞ bound on iterates S_n fail for higher dimensions (the rest of the analysis works for $d \leq 3$), but we hope it will be possible to improve these results (and possibly remove lumping altogether).

Another solution would be to use mass lumping in all nonlinear terms involving S; i.e., to use the functional

$$\begin{aligned} & \frac{\gamma}{2} \int_\Omega \left(\mathcal{I}_h\left(S^2\right) + k_\varepsilon\right) |\nabla \mathbf{U}|^2 \, d\mathbf{x} + \frac{\lambda}{2} \int_\Omega |\mathbf{U} - \mathbf{G}|^2 \, d\mathbf{x} \\ & + \alpha \int_\Omega \varepsilon |\nabla S|^2 + \frac{1}{4\varepsilon} \mathcal{I}_h\left((1-S)^2\right) d\mathbf{x}. \end{aligned}$$

This introduces additional errors, but it still allows to get the necessary uniform H^1 bounds on iterates $(\mathbf{U}_n, S_n)$, in addition to the L^∞ bound on S_n, and it does not require $d \leq 2$; see [15] for details.

Functions $\mathbf{V} \in V_h(\Omega, \mathbb{R}^m)$ which satisfy the pointwise constraint $|\mathbf{V}| = 1$ are necessarily constant. So it is more reasonable to work in the space

$$H_h^1(\mathcal{T}_h) := \left\{\mathbf{V} \in V_h(\Omega, \mathbb{R}^m) : \mathbf{V}(\mathbf{z}) \in \mathbb{S}^{m-1} \; \forall \mathbf{z} \in \mathcal{N}\right\}.$$

We set

$$K_h^n := \left\{\mathbf{W} \in V_h(\Omega, \mathbb{R}^m) : \mathbf{W}(\mathbf{z}) \cdot \mathbf{U}_n(\mathbf{z}) = 0 \; \forall \mathbf{z} \in \mathcal{N}\right\},$$

where $\mathbf{U}_n \in H_h^1(\mathcal{T}_h)$ will be the iterates of the fully discrete algorithm.

The idea now is to find $\mathbf{U} \in K_h^n$ minimising $\widetilde{E}(\cdot, S)$ and then project to the sphere. This approach is based on [1] and [5] and replaces the nonlinear, non-convex constraint $\mathbf{U} \in H_h^1(\mathcal{T}_h)$ by the linear one $\mathbf{W}(\mathbf{z}) \cdot \mathbf{U}_n(\mathbf{z}) = 0 \; \forall \mathbf{z} \in \mathcal{N}$, which in turn ensures that projection to the sphere does not increase the energy.

Algorithm 3.2. *Let a quasi-uniform triangulation $\mathcal{T}_h$ of Ω, starting values $\mathbf{U}_0, S_0$, and parameters $\varepsilon, k_\varepsilon, \varrho > 0$ be given. For $n := 0, \ldots$*

    (1) *Minimise $\widetilde{E}(\mathbf{U}_n - \mathbf{W}, S_n)$ for $\mathbf{W} \in K_h^n$; i.e. solve*

$$(3.3) \qquad \gamma\left(\left(S_n^2 + k_\varepsilon\right)\nabla\left(\mathbf{U}_n - \mathbf{W}\right), \nabla \mathbf{V}\right) - \lambda\left(\mathbf{W} + \mathbf{G}, \mathbf{V}\right) = 0,$$

        for all $\mathbf{V} \in K_h^n$, and call the solution $\mathbf{W}_n$.

    (2) *If $\|\mathbf{W}_n\|_{H^1(\Omega;\mathbb{R}^m)} \leq \varrho$ set $\mathbf{U} := \mathbf{U}_n$, $\mathbf{W} := \mathbf{W}_n$, $S := S_n$ and stop.*

    (3) *Set*

$$\mathbf{U}_{n+1} := \sum_{\mathbf{z} \in \mathcal{N}} \frac{\mathbf{U}_n(\mathbf{z}) - \mathbf{W}_n(\mathbf{z})}{|\mathbf{U}_n(\mathbf{z}) - \mathbf{W}_n(\mathbf{z})|} \boldsymbol{\varphi}_{\mathbf{z}}.$$

    (4) *Minimise $E_h(\mathbf{U}_{n+1}, S)$ for all $S \in V_h(\Omega)$; i.e. solve*

$$(3.4) \qquad 2\alpha\varepsilon\left(\nabla S, \nabla W\right) + \gamma\left(S\left|\nabla \mathbf{U}_{n+1}\right|^2, W\right) + \frac{\alpha}{2\varepsilon}\left(S - 1, W\right)_h = 0$$

        for all $W \in V_h(\Omega)$, and call the solution S_{n+1}.

Here $(\varphi, \psi)_h := \int_\Omega \mathcal{I}_h(\varphi\psi)\,\mathrm{d}\mathbf{x}$ for $\varphi, \psi \in C(\overline{\Omega})$.

Definition 3.3. *Let $\mathcal{T}_h$ be a quasi-uniform triangulation of Ω, and $s \in H^1(\Omega)$ be fixed. $\mathcal{T}_h$ is said to satisfy an* energy decreasing condition (ED) *if*

$$E_h(\mathbf{W}, s) \leq E_h(\mathbf{V}, s)$$

for all $\mathbf{V} \in V_h(\Omega, \mathbb{R}^m)$ fulfilling $|\mathbf{V}(\mathbf{z})| \geq 1$ for $\mathbf{z} \in \mathcal{N}$. Here $\mathbf{W} \in V_h(\Omega, \mathbb{R}^m)$ is defined by

$$\mathbf{W} := \sum_{\mathbf{z} \in \mathcal{N}} \frac{\mathbf{V}(\mathbf{z})}{|\mathbf{V}(\mathbf{z})|} \varphi_{\mathbf{z}}.$$

As demonstrated in [5, Lemma 3.2 & Remarks 3.3], for $d \leq 3$ (ED) is fulfilled if every angle in $\mathcal{T}_h$ is $\leq \pi/2$ (i.e., if the triangulation is *acute*).

Lemma 3.4. *Let $\mathbf{U} \in V_h(\Omega, \mathbb{R}^m)$ be given, and $d \leq 2$. If $S \in V_h(\Omega)$ minimises $E_h(\mathbf{U}, \cdot)$, then $-1 \leq S \leq 1$.*

Proof. For $a \in \mathbb{R}$ define $\overline{a} := -1 \vee a \wedge 1$. Note that for this result it is crucial that we have piecewise affine finite element functions.

    Step 1: *If $a, b \in \mathbb{R}$, then $\left(\overline{a} + \overline{b}\right)^2 \leq (a + b)^2$ and $\left(\overline{a} - \overline{b}\right)^2 \leq (a - b)^2$.*
    A case differentiation gives

- $a, b \in [-1, 1]$ is trivial.
- $a, b > 1$ or $a, b < -1 \Longrightarrow \left(\overline{a} + \overline{b}\right)^2 = 2^2 \leq (a + b)^2$.
- $a > 1, b < -1 \Longrightarrow \left(\overline{a} + \overline{b}\right)^2 = 0 \leq (a + b)^2$,
  and $b > 1, a < -1$ is symmetrical.
- $a \notin [-1, 1], b \in [-1, 1] \Longrightarrow 0 \leq 1 + \mathrm{sign}(ab)|b| \leq |a| + \mathrm{sign}(ab)|b|$,
  $\Longrightarrow \left(\overline{a} + \overline{b}\right)^2 = (1 + \mathrm{sign}(ab)|b|)^2 \leq (|a| + \mathrm{sign}(ab)|b|)^2 = (a + b)^2$,
  and $b \notin [-1, 1], a \in [-1, 1]$ is symmetrical.

Therefore $\left(\overline{a} + \overline{b}\right)^2 \leq (a + b)^2$, and $\left(\overline{a} - \overline{b}\right)^2 \leq (a - b)^2$ follows by symmetry.

    Step 2: *We have $-1 \leq S \leq 1$.*
    In case $-1 \leq S \leq 1$ should not be true, we replace $S(\mathbf{x}) = \sum_{\mathbf{z} \in \mathcal{N}} S(\mathbf{z})\varphi_{\mathbf{z}}(\mathbf{x})$ by

$$\overline{S}(\mathbf{x}) := \sum_{\mathbf{z} \in \mathcal{N}} \left(-1 \vee S(\mathbf{z}) \wedge 1\right)\varphi_{\mathbf{z}}(\mathbf{x}) = \mathcal{I}_h\left(-1 \vee S \wedge 1\right),$$

for which clearly $-1 \leq \overline{S} \leq 1$. We shall prove $E_h\left(\mathbf{U}, \overline{S}\right) \leq E_h(\mathbf{U}, S)$, by showing energy-decrease for every term involving S, on every triangle $T \in \mathcal{T}_h$. Since $\nabla \mathbf{U}$ is constant on every T, the terms we have to look at are $\int_T S^2\,\mathrm{d}\mathbf{x}$, $\int_T |\nabla S|^2\,\mathrm{d}\mathbf{x}$, and $\int_T \mathcal{I}_h\left((1 - S)^2\right)\mathrm{d}\mathbf{x}$. Let the values of S at the nodal points of T be $S_0, \ldots, S_d$, let $\overline{S}_0, \ldots, \overline{S}_d$ be the corresponding values of $\overline{S}$, let $\varphi_0, \ldots, \varphi_d$ be the corresponding nodal basis functions, and $\mathbf{x} := (x_1, \ldots, x_d)$. By a simple transformation argument, we can restrict ourselves to the standard simplex, which we shall still call T. Then

$$S(\mathbf{x})|_T = S_0 + \sum_{i=1}^d (S_i - S_0)\, x_i,$$

and
$$\nabla S(\mathbf{x})|_T = (S_1 - S_0, \ldots, S_d - S_0),$$

For the first term, a calculation yields

(3.5)
$$\int_T S^2 \mathrm{d}\mathbf{x} = \frac{2}{(d+2)!} \sum_{i=0}^{d} S_i \sum_{j=i}^{d} S_j.$$

If $d = 1$, then, by Step 1,

$$
\begin{aligned}
\int_T \overline{S}^2 \mathrm{d}\mathbf{x} &= \frac{1}{3} \left(\overline{S}_0^2 + \overline{S}_0 \overline{S}_1 + \overline{S}_1^2 \right) \\
&= \frac{1}{6} \left(\left(\overline{S}_0 + \overline{S}_1 \right)^2 + \overline{S}_0^2 + \overline{S}_1^2 \right) \\
&\leq \frac{1}{6} \left(\left(S_0 + S_1 \right)^2 + S_0^2 + S_1^2 \right) \\
&= \int_T S^2 \mathrm{d}\mathbf{x}.
\end{aligned}
$$

Similarly, if $d = 2$,

$$
\begin{aligned}
\int_T \overline{S}^2 \mathrm{d}\mathbf{x} &= \frac{1}{12} \left(\overline{S}_0^2 + \overline{S}_1^2 + \overline{S}_2^2 + \overline{S}_0 \overline{S}_1 + \overline{S}_0 \overline{S}_2 + \overline{S}_1 \overline{S}_2 \right) \\
&= \frac{1}{24} \left(\left(\overline{S}_0 + \overline{S}_1 \right)^2 + \left(\overline{S}_0 + \overline{S}_2 \right)^2 + \left(\overline{S}_1 + \overline{S}_2 \right)^2 \right) \\
&\leq \frac{1}{24} \left(\left(S_0 + S_1 \right)^2 + \left(S_0 + S_2 \right)^2 + \left(S_1 + S_2 \right)^2 \right) \\
&= \int_T S^2 \mathrm{d}\mathbf{x}.
\end{aligned}
$$

Note: Both arguments break down for $d \geq 3$; in fact, counter-examples are easy to find, c.f. Remark 3.5.

The second term gives, by Step 1 and symmetry,

$$
\begin{aligned}
\int_T |\nabla \overline{S}|^2 \mathrm{d}\mathbf{x} &= \int_T \left(\overline{S}_1 - \overline{S}_0, \ldots, \overline{S}_d - \overline{S}_0 \right)^2 \mathrm{d}\mathbf{x} \\
&= \frac{1}{d!} \left(\left(\overline{S}_1 - \overline{S}_0 \right)^2 + \cdots + \left(\overline{S}_d - \overline{S}_0 \right)^2 \right) \\
&\leq \frac{1}{d!} \left(\left(S_1 - S_0 \right)^2 + \cdots + \left(S_d - S_0 \right)^2 \right) \\
&= \int_T |\nabla S|^2.
\end{aligned}
$$

As for the last term, again by Step 1,

$$
\begin{aligned}
\int_T \mathcal{I}_h \left((1 - \overline{S})^2 \right) \mathrm{d}\mathbf{x} &= \sum_{i=1}^{d+1} \left(1 - \overline{S}_i \right)^2 \int_T \varphi_i \mathrm{d}\mathbf{x} \\
&\leq \sum_{i=1}^{d+1} \left(1 - S_i \right)^2 \int_T \varphi_i \mathrm{d}\mathbf{x} = \int_T \mathcal{I}_h \left((1 - S)^2 \right) \mathrm{d}\mathbf{x}.
\end{aligned}
$$

$\square$

Remark 3.5. *For $d = 3$, Step 2 in the above proof is wrong: Let $S_0 := S_1 := S_2 := 1$, and $S_3 := -3/2$. Then, by (3.5),*

$$\int_T \overline{S}^2 \mathrm{d}\mathbf{x} = \frac{1}{60} \sum_{i=0}^{d} \overline{S}_i \sum_{j=i}^{d} \overline{S}_j = \frac{1}{15},$$

while

$$\int_T S^2 \mathrm{d}\mathbf{x} = \frac{1}{60} \sum_{i=0}^{d} S_i \sum_{j=i}^{d} S_j = \frac{1}{16}.$$

We suspect that there exist dimension-dependent constants c_d, at which one could crop $|S|$, so that the energy is still decreasing (also replacing $(1 - s)^2$ by $(c_d - s)^2$).

Lemma 3.6. *Let $\mathcal{T}_h$ be a quasi-uniform triangulation of Ω satisfying (ED), $\varrho > 0$ fixed, $S_0 \in V_h(\Omega)$, and $\mathbf{U}_0 \in H^1_h(\mathcal{T}_h)$. Then Algorithm 3.2 terminates within a finite number of iterations with output $(\mathbf{U}, S) \in H^1_h(\mathcal{T}_h) \times V_h(\Omega, [-1, 1])$ and $\mathbf{W} \in V_h(\Omega, \mathbb{R}^m)$ such that $\|\nabla \mathbf{W}\| \leq \varrho$, and $E_h(\mathbf{U}, S) \leq E_h(\mathbf{U}_0, S_0)$.*

Proof. We proceed by induction. Suppose that for some $n \geq 0$ we have $(\mathbf{U}_n, S_n) \in H^1_h(\mathcal{T}_h) \times V_h(\Omega)$. The set K^n_h is a subspace of $V_h(\Omega, \mathbb{R}^m)$. Therefore, by Lax-Milgram, there is a unique $\mathbf{W}_n \in K^n_h$ such that (3.3) is fulfilled. Since $\mathbf{W}_n(\mathbf{z}) \cdot \mathbf{U}_n(\mathbf{z}) = 0$ and $|\mathbf{U}_n(\mathbf{z})| = 1$, we have for $\mathbf{z} \in \mathcal{N}$

$$|\mathbf{U}_n(\mathbf{z}) - \mathbf{W}_n(\mathbf{z})|^2 = 1 + |\mathbf{W}_n(\mathbf{z})|^2 \geq 1.$$

Therefore, $\mathbf{U}_{n+1}$ is well-defined and in $H^1_h(\mathcal{T}_h)$. And since $\mathbf{0} \in K^n_h$ and $\mathcal{T}_h$ fulfils (ED), we get

$$E_h(\mathbf{U}_{n+1}, S_n) \leq E_h(\mathbf{U}_n - \mathbf{W}_n, S_n).$$

Step 4 of Algorithm 3.2 has a solution S_{n+1} by convexity and coercivity of the functional. So

$$E_h(\mathbf{U}_{n+1}, S_{n+1}) \leq E_h(\mathbf{U}_{n+1}, S_n) \leq E_h(\mathbf{U}_n - \mathbf{W}_n, S_n) \leq E_h(\mathbf{U}_n, S_n).$$

In fact, $E_h(\mathbf{U}_{n+1}, S_{n+1}) \leq E_h(\mathbf{U}_{n+1}, W)$ for all $W \in V_h(\Omega)$. Therefore, by Lemma 3.4, we can assume $-1 \leq S_{n+1} \leq 1$. Furthermore,

$$
\begin{aligned}
I :=& 2\widetilde{E}(\mathbf{U}_{n+1}, S_{n+1}) - 2\widetilde{E}(\mathbf{U}_n, S_n) \\
\leq& 2\widetilde{E}(\mathbf{U}_n - \mathbf{W}_n, S_n) - 2\widetilde{E}(\mathbf{U}_n, S_n) \\
\leq& \gamma \int_\Omega \left(S^2_n + k_\varepsilon\right) \left(|\nabla \mathbf{U}_n|^2 + |\nabla \mathbf{W}_n|^2 - 2\nabla \mathbf{U}_n : \nabla \mathbf{W}_n\right) \mathrm{d}\mathbf{x} \\
&+ \lambda \int_\Omega |\mathbf{U}_n|^2 + |\mathbf{W}_n|^2 + |\mathbf{G}|^2 - 2\mathbf{G} \cdot (\mathbf{U}_n - \mathbf{W}_n) - 2\mathbf{U}_n \cdot \mathbf{W}_n \mathrm{d}\mathbf{x} \\
&- \int_\Omega \gamma \left(S^2_n + k_\varepsilon\right) |\nabla \mathbf{U}_n|^2 + \lambda \left(|\mathbf{U}_n|^2 + |\mathbf{G}|^2 - 2\mathbf{G} \cdot \mathbf{U}_n\right) \mathrm{d}\mathbf{x} \\
=& \int_\Omega \gamma \left(S^2_n + k_\varepsilon\right) \left(|\nabla \mathbf{W}_n|^2 - 2\nabla \mathbf{U}_n : \nabla \mathbf{W}_n\right) + \lambda \left(|\mathbf{W}_n|^2 + 2\mathbf{W}_n \cdot (\mathbf{G} - \mathbf{U}_n)\right) \mathrm{d}\mathbf{x}.
\end{aligned}
$$

Using equation (3.3) with $\mathbf{V} := \mathbf{W}_n$, we get

$$I \leq - \int_\Omega \gamma \left(S^2_n + k_\varepsilon\right) |\nabla \mathbf{W}_n|^2 + \lambda |\mathbf{W}_n|^2 \mathrm{d}\mathbf{x},$$

whence

$$0 \leq \frac{1}{2} \int_\Omega \gamma \left(S^2_n + k_\varepsilon\right) |\nabla \mathbf{W}_n|^2 + \lambda |\mathbf{W}_n|^2 \mathrm{d}\mathbf{x} \leq \widetilde{E}(\mathbf{U}_n, S_n) - \widetilde{E}(\mathbf{U}_{n+1}, S_{n+1}).$$

Summing this from 0 to N leads to

$$\frac{1}{2} \sum_{n=0}^N \int_\Omega \gamma \left(S^2_n + k_\varepsilon\right) |\nabla \mathbf{W}_n|^2 + \lambda |\mathbf{W}_n|^2 \mathrm{d}\mathbf{x} \leq \widetilde{E}(\mathbf{U}_0, S_0) - \widetilde{E}(\mathbf{U}_{N+1}, S_{N+1}) < +\infty;$$

i.e., the series

$$\frac{1}{2} \sum_{n \geq 0} \int_\Omega \gamma \left(S^2_n + k_\varepsilon\right) |\nabla \mathbf{W}_n|^2 + \lambda |\mathbf{W}_n|^2 \mathrm{d}\mathbf{x}$$

is convergent. Therefore, $\|\mathbf{W}_n\|_{H^1(\Omega;\mathbb{R}^m)} \leq \varrho$ for n large enough. $\qquad\square$

Theorem 3.7. *Let $\{\mathcal{T}_{h_l}\}$ be a sequence of quasi-uniform triangulations satisfying (ED) with maximal mesh size $h_l \to 0$ for $l \to +\infty$, $\varrho_l \to 0$ for $l \to +\infty$, and $E_{h_l}(\mathbf{U}_0, S_0) \leq C_0 < +\infty$ independently of h_l. Let $\{\mathbf{U}_l, S_l\}$ be the output of Algorithm 3.2 (after termination) from input $\left(\mathbf{U}^0_l, S^0_l, \varrho_l\right)$. Then the sequence $\{\mathbf{U}_l, S_l\}$ converges weakly in $H^1(\Omega, \mathbb{R}^m) \times H^1(\Omega)$ (up to subsequences, not relabelled) for $l \to +\infty$ to a point $(\mathbf{u}, s) \in H^1(\Omega, \mathbb{S}^{m-1}) \times H^1(\Omega, [-1, 1])$, with $AT_\varepsilon(\mathbf{u}, s) \leq \liminf_l AT_\varepsilon(\mathbf{U}_l, S_l) \leq \liminf_l AT_\varepsilon\left(\mathbf{U}^0_l, S^0_l\right)$.*

Proof. By assumption and Lemma 3.6, we have

$$E_{h_l}(\mathbf{U}_l, S_l) \leq E_{h_l}\left(\mathbf{U}^0_l, S^0_l\right) \leq C_0,$$

and $-1 \leq S_l \leq 1$. This implies uniform boundedness of H^1-norms of iterates $\mathbf{U}_l$ and S_l. Hence we can extract a subsequence that converges weakly in $H^1 \times H^1$ to some map $(\mathbf{u}, s)$. Poincaré's inequality (elementwise), $|\mathbf{U}_l(\mathbf{z})| = 1$ for all $\mathbf{z} \in \mathcal{N}_{h_l}$, and $|\mathbf{U}_l| \leq 1$ a.e. imply

$$\left\| |\mathbf{U}_l|^2 - 1 \right\| \leq Ch_l \left\| 2\mathbf{U}^T_l \nabla \mathbf{U}_l \right\| \leq Ch_l.$$

So $\mathbf{U}_l \to \mathbf{u}$ a.e. leads to $|\mathbf{u}| = 1$ a.e.

Since $H^1(\Omega)$ is a Hilbert space and $\{\varphi \in H^1(\Omega) : 0 \leq \varphi \leq 1 \text{ a.e}\} \subset H^1(\Omega)$ is a closed, convex set, it is weakly closed. Therefore, by the weak convergence in H^1 of $S_l \rightharpoonup s$, we get $-1 \leq s \leq 1$.

Finally, by weak lower semicontinuity of $AT_\varepsilon(\cdot, \cdot)$,

$$
\begin{aligned}
AT_\varepsilon(\mathbf{u}, s) &\leq \liminf_l AT_\varepsilon(\mathbf{U}_l, S_l) \\
&\leq \liminf_l \left(E_{h_l}(\mathbf{U}_l, S_l) + c \left\| \mathcal{I}_h\left((1 - S_l)^2 \right) - (1 - S_l)^2 \right\|_{L^1(\Omega)} \right) \\
&\leq \liminf_l \left(E_{h_l}(\mathbf{U}_l^0, S_l^0) + ch_l \|S_l\|_{L^2(\Omega)} \|\nabla S_l\|_{L^2(\Omega)} \right) \\
&\leq \liminf_l E_{h_l}(\mathbf{U}_l^0, S_l^0) \\
&\leq \liminf_l \left(AT_\varepsilon(\mathbf{U}_l^0, S_l^0) + ch_l \left\| S_l^0 \right\|_{L^2(\Omega)} \left\| \nabla S_l^0 \right\|_{L^2(\Omega)} \right) \\
&\leq \liminf_l AT_\varepsilon(\mathbf{U}_l^0, S_l^0).
\end{aligned}
$$

$\square$

Remark 3.8. *We cannot prove that* $(\mathbf{u}, s)$ *is a stationary point of* $AT_\varepsilon(\cdot, \cdot)$. *In particular, equation (3.4) in Step 4 of Algorithm 3.2 is*

$$
2\alpha\varepsilon \left(\nabla S, \nabla W \right) + \gamma \left(S \left| \nabla \mathbf{U}_{n+1} \right|^2, W \right) + \frac{\alpha}{2\varepsilon} (S - 1, W)_h = 0
$$

for all $W \in V_h(\Omega)$. *Identifying limits on a term by term basis would require identifying the limit*

$$
\lim_{n \to +\infty} \left(|\nabla \mathbf{U}_{n+1}|^2 S_n, W \right),
$$

which so far we have to leave as an open problem.

What is missing for this identification of limits is strong convergence of $\nabla \mathbf{U}_n$ *in* L^2. *This is a fundamental shortcoming also observed in* [1, 5] *for the simpler case of harmonic maps to the sphere. In fact, we are not aware of any algorithm, even in the harmonic mapping case, that simultaneously gives strong convergence of* $\nabla \mathbf{U}_n$ *in* L^2 *and assures the sphere constraint* exactly.

However, the algorithm converges, decreases the energy, assures the sphere constraint exactly and delivers very convincing computational results (indeed, it is faster and delivers better results than the alternative algorithm described in the sequel, c.f. Section 6).

4. Γ-Convergence for Penalisation & Splitting

In order to resolve the problems with passing to the limit, we now use a penalisation approach instead of projection. This requires adding a term to the Ambrosio-Tortorelli energy, which penalises the sphere constraint. In this section, we show that this addition does not affect Γ-convergence to the Mumford-Shah functional, if the penalisation term is properly scaled.

Let $\Omega \subset \mathbb{R}^d$, γ, α, λ be fixed positive constants, $\varepsilon, \delta_\varepsilon > 0$, $k_\varepsilon \geq 0$, $\mathbf{g} \in L^\infty(\Omega, \mathbb{S}^{m-1})$, and $G_\varepsilon, G : L^2(\Omega, \mathbb{R}^m) \times L^2(\Omega) \to [0, +\infty]$ be defined by

$$
G_\varepsilon(\mathbf{u}, s) := \begin{cases} \dfrac{\gamma}{2} \displaystyle\int_\Omega \left(s^2 + k_\varepsilon \right) |\nabla \mathbf{u}|^2 \mathrm{d}\mathbf{x} + \dfrac{\lambda}{2} \displaystyle\int_\Omega |\mathbf{u} - \mathbf{g}|^2 \mathrm{d}\mathbf{x} & \text{if } \mathbf{u} \in H^1(\Omega, \mathbb{R}^m), \\[2mm] \quad + \alpha \displaystyle\int_\Omega \left(\varepsilon |\nabla s|^2 + \dfrac{(1 - s)^2}{4\varepsilon} \right) \mathrm{d}\mathbf{x} & s \in H^1(\Omega, [0, 1]), \\[2mm] \quad + \dfrac{1}{4\delta_\varepsilon} \displaystyle\int_\Omega \left(|\mathbf{u}|^2 - 1 \right)^2 \mathrm{d}\mathbf{x} & \\[2mm] +\infty, & \text{otherwise,} \end{cases}
$$

and

$$
G(\mathbf{u}, s) := \begin{cases} \dfrac{\gamma}{2} \displaystyle\int_\Omega |\nabla \mathbf{u}|^2 \mathrm{d}\mathbf{x} + \alpha \mathcal{H}^{d-1}(S_{\mathbf{u}}) + \dfrac{\lambda}{2} \displaystyle\int_\Omega |\mathbf{u} - \mathbf{g}|^2 \mathrm{d}\mathbf{x} & \text{if } \mathbf{u} \in GSBV(\Omega, \mathbb{S}^{m-1}) \\[2mm] & \text{and } s = 1 \text{ a.e.} \\[2mm] +\infty, & \text{otherwise.} \end{cases}
$$

Theorem 4.1. *If $\Omega \subset \mathbb{R}^d$ is open and bounded with Lipschitz boundary, $\delta_\varepsilon \xrightarrow[\varepsilon \to 0]{} 0$, $k_\varepsilon = o(\varepsilon)$, and $k_\varepsilon = o(\delta_\varepsilon)$, then $G_\varepsilon \xrightarrow[\varepsilon \to 0]{\Gamma} G$ in $L^2(\Omega, \mathbb{R}^m) \times L^2(\Omega)$.*

Moreover, there exists a solution $\{\mathbf{u}_\varepsilon, s_\varepsilon\}$ to the minimum problem

$$m_\varepsilon = \inf_{\substack{\mathbf{u} \in H^1(\Omega, \mathbb{R}^m), \\ s \in H^1(\Omega, [0,1])}} G_\varepsilon(\mathbf{u}, s)$$

with $\|\mathbf{u}_\varepsilon\|_{L^\infty} \leq C$, and every cluster point of $\{\mathbf{u}_\varepsilon\}$ is a solution to the minimum problem

$$m = \inf_{\mathbf{u} \in GSBV(\Omega, \mathbb{S}^{m-1})} G(\mathbf{u}, 1),$$

and $m_\varepsilon \to m$ as $\varepsilon \to 0^+$.

For the $\liminf$ inequality we can apply the work of Focardi ([32, Lemma 3.3]). For the $\limsup$ inequality we use the same construction as Ambrosio and Tortorelli in [3], so it is enough to verify that the penalisation term we added vanishes for $\varepsilon \to 0^+$. This is explained in more detail below.

Proof. For notational convenience, we first localise the functionals above, denoting by $G_\varepsilon(\mathbf{u}, s, A)$ and $G(\mathbf{u}, s, A)$ the same functionals with integration over $A \subseteq \Omega$ instead of Ω, and $\mathcal{H}^{d-1}(S_{\mathbf{u}})$ replaced by $\mathcal{H}^{d-1}(S_{\mathbf{u}} \cap A)$.

Step 1: *The Liminf Inequality.*

Let $\varepsilon \to 0^+$, and $(\mathbf{u}_\varepsilon, s_\varepsilon) \to (\mathbf{u}, s)$ in $L^2(\Omega, \mathbb{R}^m) \times L^2(\Omega)$. Up to subsequences, we can suppose that $(\mathbf{u}_\varepsilon, s_\varepsilon) \to (\mathbf{u}, s)$ a.e., and that $\lim_{\varepsilon \to 0^+} G_\varepsilon(\mathbf{u}_\varepsilon, s_\varepsilon)$ exists and is finite. We can further assume $s = 1$ a.e., since otherwise $\int_\Omega (1 - s_\varepsilon)^2 \, d\mathbf{x} \nrightarrow 0$, and $G_\varepsilon(\mathbf{u}_\varepsilon, s_\varepsilon) \to \infty$. Similarly, we get $|\mathbf{u}|^2 = 1$ a.e.

We now have to show

$$\liminf_{\varepsilon \to 0^+} G_\varepsilon(\mathbf{u}_\varepsilon, s_\varepsilon) \geq G(\mathbf{u}, s).$$

Since it is clear that $\int_\Omega |\mathbf{u}_\varepsilon - \mathbf{g}|^2 \, d\mathbf{x} \to \int_\Omega |\mathbf{u} - \mathbf{g}|^2 \, d\mathbf{x}$, and that the penalisation term is non-negative, it is sufficient to prove that $\mathbf{u} \in GSBV(\Omega, \mathbb{R}^m)$, and

$$\liminf_{\varepsilon \to 0^+} \int_\Omega \left(s_\varepsilon^2 + k_\varepsilon \right) |\nabla \mathbf{u}_\varepsilon|^2 \, d\mathbf{x} + 2 \int_\Omega \left(\varepsilon |\nabla s_\varepsilon|^2 + \frac{(1 - s_\varepsilon)^2}{4\varepsilon} \right) d\mathbf{x}$$

$$\geq \int_\Omega |\nabla \mathbf{u}|^2 d\mathbf{x} + 2\mathcal{H}^{d-1}(S_{\mathbf{u}}).$$

This was shown for a more general situation in [32, Lemma 3.3] (see also [33]).

Step 2: *The Limsup Inequality.*

It suffices to consider the case $\mathbf{u} \in SBV(\Omega, \mathbb{R}^m) \cap L^\infty(\Omega, \mathbb{R}^m)$. We can also assume $\nabla \mathbf{u} \in L^2(\Omega, \mathbb{R}^{d \times m})$, $|\mathbf{u}|^2 = 1$ a.e., and (see [33, Theorem 2.7.14]) that $S_{\mathbf{u}}$ is essentially closed in Ω; i.e., $\mathcal{H}^{d-1}(\Omega \cap (\overline{S_{\mathbf{u}}} \setminus S_{\mathbf{u}})) = 0$. Setting $d(\mathbf{x}) := \text{dist}(\mathbf{x}, S_{\mathbf{u}})$, we define the *Minkowski content* of $S_{\mathbf{u}}$

$$\mathcal{M}^{d-1}(S_{\mathbf{u}}) := \lim_{\delta \to 0^+} \mathcal{M}^{d-1}_\delta(S_{\mathbf{u}}) := \lim_{\delta \to 0^+} \frac{|\{\mathbf{x} \in \Omega : d(\mathbf{x}) < \delta\}|}{2\delta}.$$

It is well-known that for $S_{\mathbf{u}}$ essentially closed,

$$(4.1) \qquad\qquad \lim_{\delta \to 0^+} \mathcal{M}^{d-1}_\delta(S_{\mathbf{u}}) = \mathcal{H}^{d-1}(S_{\mathbf{u}})$$

(see [31, Theorem 3.2.39]). So, there exists a sequence $w_\varepsilon \to 0^+$, such that

$$(4.2) \qquad\qquad |\{\mathbf{x} \in \Omega : d(\mathbf{x}) < \delta\}| \leq 2\delta \left(\mathcal{H}^{d-1}(S_{\mathbf{u}}) + w_\varepsilon \right),$$

for every $\delta \geq 0$ small enough.

Given such functions $\mathbf{u}$, and $s = 1$ a.e., we have to construct $\{\mathbf{u}_\varepsilon, s_\varepsilon\}$ that converge in $L^2(\Omega, \mathbb{R}^m) \times L^2(\Omega)$ to $(\mathbf{u}, s)$, such that

$$\limsup_{\varepsilon \to 0^+} G_\varepsilon(\mathbf{u}_\varepsilon, s_\varepsilon) \leq G(u, s)$$

for any positive sequence ε converging to zero.

It is natural to require $s_\varepsilon \equiv 0$ in some ε-dependent neighbourhood of $S_{\mathbf{u}}$, s_ε converging to 1 everywhere outside a larger neighbourhood of $S_{\mathbf{u}}$, and smooth in between, as well as $\mathbf{u}_\varepsilon \equiv \mathbf{u}$ everywhere outside some neighbourhood of $S_{\mathbf{u}}$.

To this end, we use the same construction as in the paper [3] by Ambrosio and Tortorelli: Choose a positive sequence b_ε, such that $b_\varepsilon = o(\varepsilon)$, $b_\varepsilon = o(\delta_\varepsilon)$, and $k_\varepsilon = o(b_\varepsilon)$. For any $b > 0$, set $S_b := \{\mathbf{x} \in \Omega : d(\mathbf{x}) < b\}$. Thanks to (4.2), $|S_b| = O(b)$. For $t \geq b_\varepsilon$, let

$$\begin{aligned} \sigma_\varepsilon(t) &:= 1 - \exp\left(-\frac{t - b_\varepsilon}{2\varepsilon}\right), \text{ so that} \\ \sigma'_\varepsilon(t) &= \frac{1}{2\varepsilon}\exp\left(-\frac{t - b_\varepsilon}{2\varepsilon}\right). \end{aligned}$$

We now set (c.f. Figure 1)

(4.3)
$$s_\varepsilon(\mathbf{x}) := \begin{cases} 0 & \text{if } \mathbf{x} \in S_{b_\varepsilon}, \\ \sigma_\varepsilon(d(\mathbf{x})) & \text{if } \mathbf{x} \in S_{b_\varepsilon + 2\varepsilon \ln \frac{1}{\varepsilon}} \setminus S_{b_\varepsilon}, \\ 1 - \varepsilon & \text{if } \mathbf{x} \in \Omega \setminus S_{b_\varepsilon + 2\varepsilon \ln \frac{1}{\varepsilon}}, \end{cases}$$

and

$$\mathbf{u}_\varepsilon(\mathbf{x}) := \mathbf{u}(\mathbf{x}) \min\left\{\frac{d(\mathbf{x})}{b_\varepsilon}, 1\right\}.$$

Note that $0 < 2\varepsilon \ln \frac{1}{\varepsilon} \to 0^+$, and $\varepsilon = o\left(2\varepsilon \ln \frac{1}{\varepsilon}\right)$.
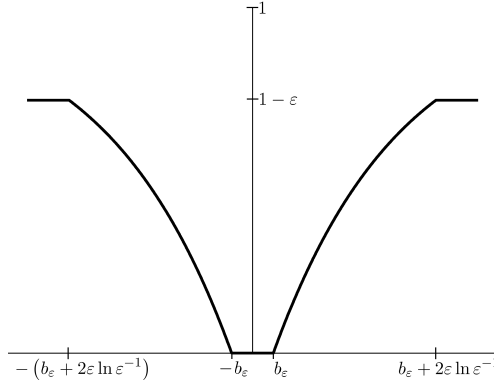
FIGURE 1. Sketch of $s_\varepsilon(\mathbf{x})$ in the case $S_{\mathbf{u}} = \{0\}$, and $d = 1$.

By construction, $(\mathbf{u}_\varepsilon, s_\varepsilon) \to (\mathbf{u}, 1)$ in $L^2(\Omega, \mathbb{R}^m) \times L^2(\Omega)$, as $\varepsilon \to 0^+$.

Therefore, we have for the term penalising the sphere constraint,

(4.4)
$$\frac{1}{4\delta_\varepsilon}\int_\Omega \left(|\mathbf{u}_\varepsilon|^2 - 1\right)^2 \mathrm{d}\mathbf{x} \leq c\frac{|S_{b_\varepsilon}|}{\delta_\varepsilon} \leq c\frac{b_\varepsilon}{\delta_\varepsilon} \to 0.$$

So this term does not contribute to the lim sup. This calculation motivates why we cannot expect good experimental results for δ_ε too small (compared to b_ε, which in turn is between ε and k_ε); i.e., we have to sacrifice something in terms of the sphere constraint, c.f. our experiments in Section 6.2.

The other terms are just like in the original paper [3].

Step 3: *Convergence of Minimisers.*

The functional G_ε is coercive and lower semicontinuous in L^2. So for every $\varepsilon > 0$ there exists a minimising pair $(\mathbf{u}_\varepsilon, s_\varepsilon)$ of G_ε. By a simple truncation argument, $\|\mathbf{u}_\varepsilon\|_{L^\infty} \leq C$. As above, we can assume that $(\mathbf{u}_\varepsilon, s_\varepsilon) \in SBV(\Omega, \mathbb{R}^m) \times SBV(\Omega) \cap L^\infty(\Omega, \mathbb{R}^m) \times L^\infty(\Omega)$. By the SBV Closure and Compactness Theorems [2, Theorems 4.7 and 4.8], there exists a subsequence $\{\mathbf{u}_{\varepsilon_j}, s_{\varepsilon_j}\}$ converging to some $(\mathbf{u}, 1)$ in $L^2(\Omega, \mathbb{R}^m) \times L^2(\Omega)$, with $\mathbf{u} \in SBV(\Omega, \mathbb{R}^m)$. Thus, the stability of minimising sequences under Γ-convergence (Lemma 2.1(3)) concludes the proof. $\qquad\square$

5. Penalisation & Splitting Algorithm

Let $\Omega \subset \mathbb{R}^d$, be a polyhedral Lipschitz domain, and let $\mathbf{g} : \Omega \to \mathbb{S}^{m-1}$ be the chromaticity component of a given image. For $\mathbf{u}, \mathbf{g} \in H^1(\Omega, \mathbb{R}^m)$, $s \in H^1(\Omega, [0, 1])$, and $0 < \varepsilon, k_\varepsilon, \delta_\varepsilon \ll 1$, we want to minimise

the following vector valued Ambrosio-Tortorelli-Ginzburg-Landau energy using a splitting strategy:

$$(5.1) \qquad \begin{aligned} G_\varepsilon(\mathbf{u}, s) &= \frac{\gamma}{2} \int_\Omega \left(s^2 + k_\varepsilon\right) |\nabla \mathbf{u}|^2 \, \mathrm{d}\mathbf{x} + \frac{\lambda}{2} \int_\Omega |\mathbf{u} - \mathbf{g}|^2 \, \mathrm{d}\mathbf{x} \\ &\quad + \alpha \int_\Omega \varepsilon \, |\nabla s|^2 + \frac{1}{4\varepsilon}(1-s)^2 \mathrm{d}\mathbf{x} + \frac{1}{4\delta_\varepsilon} \int_\Omega \left(|\mathbf{u}|^2 - 1\right)^2 \mathrm{d}\mathbf{x}. \end{aligned}$$

In this section, we shall always assume $\gamma, \alpha, \varepsilon, k_\varepsilon, \delta_\varepsilon$ to be fixed and positive, $\lambda \geq 0$, and $d \leq 2$ (the last assumption is again only used to show that iterates $S_n \in [-1, 1]$, and that their weak limit $s \in [0, 1]$).

Definition 5.1. *A tuple* $(\mathbf{u}, s) \in H^1(\Omega, \mathbb{R}^m) \times H^1(\Omega, [0, 1])$ *is called a* weak solution *to the problem* $\inf G_\varepsilon$, *if and only if*

$$(5.2) \qquad \gamma\left(\left(s^2 + k_\varepsilon\right) \nabla \mathbf{u}, \nabla \boldsymbol{\varphi}\right) + \lambda\left(\mathbf{u} - \mathbf{g}, \boldsymbol{\varphi}\right) + \frac{1}{\delta_\varepsilon}\left(\left(|\mathbf{u}|^2 - 1\right)\mathbf{u}, \boldsymbol{\varphi}\right) = 0$$

for all $\boldsymbol{\varphi} \in H^1(\Omega, \mathbb{R}^m)$, *and*

$$(5.3) \qquad 2\alpha\varepsilon\left(\nabla s, \nabla \varphi\right) + \gamma\left(|\nabla \mathbf{u}|^2 s, \varphi\right) + \frac{\alpha}{2\varepsilon}\left(s - 1, \varphi\right) = 0$$

for all $\varphi \in H^1(\Omega) \cap L^\infty(\Omega)$.

We use the same finite element setting as in Section 3, in particular, we shall always assume the triangulation $\mathcal{T}_h$ to be quasi-uniform. For $\mathbf{U}, \mathbf{G} \in V_h(\Omega, \mathbb{R}^m)$ and $S \in V_h(\Omega, [-1, 1])$, let

$$(5.4) \qquad \begin{aligned} G_{\varepsilon,h}(\mathbf{U}, S) &= \frac{\gamma}{2} \int_\Omega \left(S^2 + k_\varepsilon\right) |\nabla \mathbf{U}|^2 \, \mathrm{d}\mathbf{x} + \frac{\lambda}{2} \int_\Omega |\mathbf{U} - \mathbf{G}|^2 \, \mathrm{d}\mathbf{x} \\ &\quad + \alpha \int_\Omega \varepsilon \, |\nabla S|^2 + \frac{1}{4\varepsilon}\mathcal{I}_h\left((1-S)^2\right) \mathrm{d}\mathbf{x} + \frac{1}{4\delta_\varepsilon} \int_\Omega \left(|\mathbf{U}|^2 - 1\right)^2 \mathrm{d}\mathbf{x}. \end{aligned}$$

In the algorithm below we use $\mathbf{G} := \mathbf{r}_h(\mathbf{g}) \in V_h(\Omega, \mathbb{R}^m)$, i.e., the Clément interpolation of $\mathbf{g}$. This allows the use of non-smooth $\mathbf{g}$. If $\mathbf{g} \in C^0(\Omega, \mathbb{R}^m)$, the Lagrange interpolation would do as well.

Algorithm 5.2. *Let* $\mathbf{U}_0, \mathbf{G} \in V_h(\Omega, \mathbb{R}^m)$ *and* $S_0 \in V_h(\Omega)$ *be given. For* $n = 1, \dots$ *until convergence do*
   (1) *Compute* $\mathbf{U}_n \in V_h(\Omega, \mathbb{R}^m)$ *such that*

$$(5.5) \qquad \gamma\left(\left(S_{n-1}^2 + k_\varepsilon\right) \nabla \mathbf{U}_n, \nabla \mathbf{W}\right) + \lambda\left(\mathbf{U}_n - \mathbf{G}, \mathbf{W}\right) + \frac{1}{\delta_\varepsilon}\left(\left(|\mathbf{U}_n|^2 - 1\right)\mathbf{U}_n, \mathbf{W}\right) = 0$$

   for all $\mathbf{W} \in V_h(\Omega, \mathbb{R}^m)$.
   (2) *Compute* $S_n \in V_h(\Omega)$ *such that*

$$(5.6) \qquad 2\alpha\varepsilon\left(\nabla S_n, \nabla W\right) + \gamma\left(S_n |\nabla \mathbf{U}_n|^2, W\right) + \frac{\alpha}{2\varepsilon}\left(S_n - 1, W\right)_h = 0$$

   for all $W \in V_h(\Omega)$.

We start with a discussion of relevant stability properties of iterates from Algorithm 5.2.

Lemma 5.3. *Algorithm 5.2 decreases* $G_{\varepsilon,h}$ *with respect to* $n \in \mathbb{N}$.

Proof. For any $n \in \mathbb{N}$ fixed, Algorithm 5.2 ensures, that

$$G_{\varepsilon,h}(\mathbf{U}_{n+1}, S_{n+1}) \leq G_{\varepsilon,h}(\mathbf{U}_{n+1}, S_n) \leq G_{\varepsilon,h}(\mathbf{U}_n, S_n).$$

$\square$

The following existence and uniqueness result follows by standard coercivity and convexity arguments for $G_{\varepsilon,h}$ (see e.g. [34, Section 8.4]). The fact $-1 \leq S \leq 1$ follows from Lemma 3.4.

Proposition 5.4. *There exists a function* $\mathbf{U} \in V_h(\Omega, \mathbb{R}^m)$, *such that equation* (5.5) *holds for all* $\mathbf{W} \in V_h(\Omega, \mathbb{R}^m)$, *and a unique function* $S \in V_h(\Omega, [-1, 1])$, *such that equation* (5.6) *holds for all* $W \in V_h(\Omega)$.

Main convergence properties of iterates from Algorithm 5.2 are given in the following

Theorem 5.5. *Let* $\{\mathcal{T}_{h_l}\}$ *be a sequence of quasi-uniform triangulations with maximal mesh size* $h_l \to 0$ *for* $l \to +\infty$, *and* $G_{\varepsilon,h_l}\left(\mathbf{U}_0^l, S_0^l\right) \leq C_0 < +\infty$ *independently of* h_l. *Then the sequences* $\left\{\mathbf{U}_m^l, S_m^l\right\}_{m,l}$, *constructed by Algorithm 5.2 from inputs* $\left(\mathbf{U}_0^l, S_0^l\right)$ *have a (diagonal) subsequence called* $\{\mathbf{U}_n, S_n\}_n$, *such that* $\mathbf{U}_n$ *converges strongly in* $H^1(\Omega, \mathbb{R}^m)$, *and* S_n *converges weakly in* $H^1(\Omega)$ *to some* $(\mathbf{u}, s) \in H^1(\Omega, \mathbb{R}^m) \times H^1(\Omega, [0, 1])$, *which is a weak solution as in Definition 5.1.*

For identifying limits in the proof of Theorem 5.5, it will be crucial to prove strong L^2 convergence of $\nabla \mathbf{U}_n$ to $\nabla \mathbf{u}$, for which we use a strategy derived from [15, Proof of Theorem 2], where the authors show convergence of two adaptive, stationary finite element approximations for the minimisation of the unconstrained Ambrosio-Tortorelli energy: In Step 2 we show that $\mathbf{u}$ fulfils equation (5.2), then we use equations (5.2) and (5.5) and dominated convergence (c.f. Lemma 5.6, also derived from [15]) to show strong L^2 convergence of $\nabla \mathbf{U}_n$ to $\nabla \mathbf{u}$ in Step 3, and finally we use this to show that s fulfils equation (5.3) in Step 4.

Lemma 5.6. *Let $p_n, p \in H^1(\Omega) \cap L^\infty(\Omega)$, such that $\|p_n\|_{L^\infty(\Omega)}, \|p\|_{L^\infty(\Omega)} \leq C < +\infty$ a.e., independently of n, and $p_n \to p$ in $L^2(\Omega)$. Then*

$$\lim_n \left(|p_n - p|, |\nabla \boldsymbol{\varphi}|^2 \right) = 0 \qquad \forall \boldsymbol{\varphi} \in H^1(\Omega, \mathbb{R}^m).$$

Proof. See [15, Proof of Theorem 2]. $\qquad\qquad\qquad\qquad\qquad\qquad\qquad\qquad\qquad\qquad\qquad\qquad$ $\square$

Proof of Theorem 5.5. **Step 1:** *For $m, l \to \infty$, there is a subsequence $\{\mathbf{U}_n, S_n\}$, converging weakly in $H^1(\Omega, \mathbb{R}^m) \times H^1(\Omega)$ to some $(\mathbf{u}, s) \in H^1(\Omega, \mathbb{R}^m) \times H^1(\Omega, [-1, 1])$.*

For every $m, l \in \mathbb{N}$, Proposition 5.4 gives existence of $\left(\mathbf{U}_m^l, S_m^l \right)$ and ensures that $-1 \leq S_m^l \leq 1$ a.e. By Lemma 5.3 and by assumption,

$$G_{\varepsilon, h_l} \left(\mathbf{U}_m^l, S_m^l \right) \leq G_{\varepsilon, h_l} \left(\mathbf{U}_0^l, S_0^l \right) \leq C_0,$$

independently of l, m. In particular, $G_{\varepsilon, h_n}(\mathbf{U}_n^n, S_n^n) \leq C_0$. So, by the definition of G_{ε, h_n}, the H^1-norms of $\mathbf{U}_n^n$ and S_n^n are bounded independently of n. Therefore, since H^1 is a Hilbert space, there exist subsequences, called $\{\mathbf{U}_n\}$ and $\{S_n\}$, which converge weakly in H^1 to some $(\mathbf{u}, s) \in H^1(\Omega, \mathbb{R}^m) \times H^1(\Omega)$.

Finally, since $H^1(\Omega)$ is a Hilbert space and $\{\varphi \in H^1(\Omega) : -1 \leq \varphi \leq 1 \text{ a.e}\} \subset H^1(\Omega)$ is a closed, convex set, it is weakly closed. Therefore, by the weak convergence in H^1 of $S_n \rightharpoonup s$, we get $-1 \leq s \leq 1$.

Below, we shall use the abbreviation h for h_n.

Step 2: $\mathbf{u}$ *solves equation* (5.2).
Let $\boldsymbol{\varphi} \in C^\infty(\Omega, \mathbb{R}^m)$ be fixed, $n \in \mathbb{N}$, and $h > 0$. Consider

$$\gamma \left(\left(s^2 + k_\varepsilon \right) \nabla \mathbf{u}, \nabla \boldsymbol{\varphi} \right) + \lambda \left(\mathbf{u} - \mathbf{g}, \boldsymbol{\varphi} \right) + \frac{1}{\delta_\varepsilon} \left(\left(|\mathbf{u}|^2 - 1 \right) \mathbf{u}, \boldsymbol{\varphi} \right) =: \gamma T_1 + \lambda T_2 + \frac{1}{\delta_\varepsilon} T_3.$$

Since H^1 is compactly embedded in L^p for $p < 6$, as long as the space dimension $d \leq 3$, we have $\mathbf{U}_n \to \mathbf{u}$ in $L^p(\Omega, \mathbb{R}^m)$ for $p < 6$.

We compute

$$
\begin{aligned}
T_1 &= \left(\left(S_{n-1}^2 + k_\varepsilon \right) \nabla \mathbf{U}_n, \nabla \boldsymbol{\mathcal{I}}_h(\boldsymbol{\varphi}) \right) + \left(\left(s^2 - S_{n-1}^2 \right) \nabla \mathbf{U}_n, \nabla \boldsymbol{\varphi} \right) \\
&\quad + \left(\left(s^2 + k_\varepsilon \right) \nabla \left(\mathbf{u} - \mathbf{U}_n \right), \nabla \boldsymbol{\varphi} \right) + \left(\left(S_{n-1}^2 + k_\varepsilon \right) \nabla \mathbf{U}_n, \nabla \left(\boldsymbol{\varphi} - \boldsymbol{\mathcal{I}}_h(\boldsymbol{\varphi}) \right) \right) \\
&=: T_{11}^n + T_{12}^n + T_{13}^n + T_{14}^n.
\end{aligned}
$$

Note that $\|\boldsymbol{\varphi} - \boldsymbol{\mathcal{I}}_h(\boldsymbol{\varphi})\|_{H^r(\Omega, \mathbb{R}^m)} \leq ch^{2-r} \|\nabla^2 \boldsymbol{\varphi}\|_{L^2(\Omega, \mathbb{R}^m)}$ for $0 \leq r \leq 2$.

Since $-1 \leq S_{n-1}, s \leq 1$, we have $\left| S_{n-1}^2 - s^2 \right| \leq C |S_{n-1} - s| \leq C |S_{n-1} - s|^{1/2}$, whence, by Lemma 5.6,

$$T_{12}^n = \left(\left(s^2 - S_{n-1}^2 \right) \nabla \mathbf{U}_n, \nabla \boldsymbol{\varphi} \right) \leq C \left(|s - S_{n-1}|, |\nabla \boldsymbol{\varphi}|^2 \right)^{1/2} \|\nabla \mathbf{U}_n\|_{L^2(\Omega, \mathbb{R}^{m \times d})} \xrightarrow[n \to +\infty]{h \to 0} 0.$$

Since $s \leq 1$, we know that $\left(s^2 + k_\varepsilon \right) \nabla \boldsymbol{\varphi} \in L^2\left(\Omega, \mathbb{R}^{d \times m} \right)$, so $T_{13}^n = \left(\nabla \left(\mathbf{u} - \mathbf{U}_n \right), \left(s^2 + k_\varepsilon \right) \nabla \boldsymbol{\varphi} \right) \to 0$, by weak convergence. And since $\|\boldsymbol{\varphi} - \boldsymbol{\mathcal{I}}_h(\boldsymbol{\varphi})\|_{H^1(\Omega, \mathbb{R}^m)} \to 0$, using the bounds established in Step 1, the terms T_{14}^n, T_2, T_3 all clearly vanish.

Putting all of the above together, we have for $n \in \mathbb{N}$ and $h > 0$ fixed,

$$\gamma \left(\left(s^2 + k_\varepsilon \right) \nabla \mathbf{u}, \nabla \boldsymbol{\varphi} \right) + \lambda \left(\mathbf{u} - \mathbf{g}, \boldsymbol{\varphi} \right) + \frac{1}{\delta_\varepsilon} \left(\left(|\mathbf{u}|^2 - 1 \right) \mathbf{u}, \boldsymbol{\varphi} \right) =: \gamma T_{13}^n + \lambda T_{21}^n + \frac{1}{\delta_\varepsilon} T_{31}^n + T^n,$$

where $\gamma T_{13}^n + \lambda T_{21}^n + \frac{1}{\delta_\varepsilon} T_{31}^n = 0$ by construction. Now, letting $n \to +\infty$ and $h \to 0$, we have $T^n \to 0$, as shown above. And by a density argument, the above is true for general $\boldsymbol{\varphi} \in H^1(\Omega, \mathbb{R}^m)$.

Step 3: $\nabla \mathbf{U}_n \to \nabla \mathbf{u}$ *strongly in* $L^2\left(\Omega, \mathbb{R}^{m \times d} \right)$, *as* $n \to +\infty$ *and* $h \to 0$.

Let $n \in \mathbb{N}$ and $h > 0$. Then

$$
\begin{aligned}
\gamma k_\varepsilon &\left\| \nabla \left(\mathbf{u} - \mathbf{U}_n \right) \right\|_{L^2}^2 \\
&\leq \gamma \left(\left(S_{n-1}^2 + k_\varepsilon \right) \nabla \mathbf{u}, \nabla \left(\mathbf{R}_h(\mathbf{u}) - \mathbf{U}_n \right) \right) \\
&\quad - \gamma \left(\left(S_{n-1}^2 + k_\varepsilon \right) \nabla \mathbf{U}_n, \nabla \left(\mathbf{R}_h(\mathbf{u}) - \mathbf{U}_n \right) \right) \\
&\quad - \lambda \left(\mathbf{U}_n - \mathbf{G}, \mathbf{R}_h(\mathbf{u}) - \mathbf{U}_n \right) - \frac{1}{\delta_\varepsilon} \left(\left(\left| \mathbf{U}_n \right|^2 - 1 \right) \mathbf{U}_n, \mathbf{R}_h(\mathbf{u}) - \mathbf{U}_n \right) \\
&\quad + \lambda \left(\mathbf{U}_n - \mathbf{G}, \mathbf{R}_h(\mathbf{u}) - \mathbf{U}_n \right) + \frac{1}{\delta_\varepsilon} \left(\left(\left| \mathbf{U}_n \right|^2 - 1 \right) \mathbf{U}_n, \mathbf{R}_h(\mathbf{u}) - \mathbf{U}_n \right) \\
&\quad + \gamma \left(\left(S_{n-1}^2 + k_\varepsilon \right) \nabla \left(\mathbf{u} - \mathbf{U}_n \right), \nabla \left(\mathbf{u} - \mathbf{R}_h(\mathbf{u}) \right) \right) \\
&=: T_1^n + \ldots + T_7^n.
\end{aligned}
$$

By construction (equation (5.5) with $\mathbf{W} := \mathbf{R}_h(\mathbf{u}) - \mathbf{U}_n$), the expression $T_2^n + T_3^n + T_4^n$ is zero.

$$
\begin{aligned}
T_1^n &= \gamma \left(\left(S_{n-1}^2 - s^2 \right) \nabla \mathbf{u}, \nabla \left(\mathbf{R}_h(\mathbf{u}) - \mathbf{U}_n \right) \right) + \gamma \left(\left(s^2 + k_\varepsilon \right) \nabla \mathbf{u}, \nabla \left(\mathbf{R}_h(\mathbf{u}) - \mathbf{U}_n \right) \right) \\
&\quad + \lambda \left(\mathbf{u} - \mathbf{g}, \mathbf{R}_h(\mathbf{u}) - \mathbf{U}_n \right) + \frac{1}{\delta_\varepsilon} \left(\left(\left| \mathbf{u} \right|^2 - 1 \right) \mathbf{u}, \mathbf{R}_h(\mathbf{u}) - \mathbf{U}_n \right) \\
&\quad - \lambda \left(\mathbf{u} - \mathbf{g}, \mathbf{R}_h(\mathbf{u}) - \mathbf{U}_n \right) - \frac{1}{\delta_\varepsilon} \left(\left(\left| \mathbf{u} \right|^2 - 1 \right) \mathbf{u}, \mathbf{R}_h(\mathbf{u}) - \mathbf{U}_n \right) \\
&=: T_{11}^n + \ldots + T_{16}^n.
\end{aligned}
$$

By Step 2, $T_{12}^n + T_{13}^n + T_{14}^n = 0$. Therefore

$$
\gamma k_\varepsilon \left\| \nabla \left(\mathbf{u} - \mathbf{U}_n \right) \right\|_{L^2}^2 \leq T_{11}^n + T_{15}^n + T_{16}^n + T_5^n + T_6^n + T_7^n.
$$

All of the above is true for any $n \in \mathbb{N}$. Now, consider the limit $n \to +\infty$ and $h \to 0$. Note that, by a density-argument,

$$
\left\| \mathbf{R}_h(\mathbf{u}) - \mathbf{U}_n \right\|_X \leq \left\| \mathbf{R}_h(\mathbf{u}) - \mathbf{u} \right\|_X + \left\| \mathbf{u} - \mathbf{U}_n \right\|_X \xrightarrow[n \to +\infty]{h \to 0} 0,
$$

for $X = H^1$ and, by embedding, $X = L^p$ ($p < 6$). Therefore we have, similarly to Step 2, that the terms $T_5^n, T_6^n, T_7^n, T_{15}^n$ and T_{16}^n all vanish in the limit $h \to 0$ and $n \to +\infty$. Finally, T_{11}^n vanishes using Lemma 5.6, as in Step 2, and the H^1-stability of the Ritz projection.

Step 4: *s solves equation (5.3), and $0 \leq s \leq 1$.*

Let $\varphi \in C^\infty(\Omega)$ be fixed, $n \in \mathbb{N}$, and $h > 0$. Set

$$
2\alpha\varepsilon \left(\nabla s, \nabla \varphi \right) + \gamma \left(\left| \nabla \mathbf{u} \right|^2 s, \varphi \right) + \frac{\alpha}{2\varepsilon} \left(s - 1, \varphi \right) := 2\alpha\varepsilon T_1 + \gamma T_2 + \frac{\alpha}{2\varepsilon} T_3.
$$

We have

$$
\begin{aligned}
T_1 &= \left(\nabla S_n, \nabla \mathcal{I}_h(\varphi) \right) + \left(\nabla S_n, \nabla \left(\varphi - \mathcal{I}_h(\varphi) \right) \right) + \left(\nabla \left(s - S_n \right), \nabla \varphi \right) \\
&=: T_{11}^n + T_{12}^n + T_{13}^n,
\end{aligned}
$$

with $T_{12}^n, T_{13}^n \to 0$ by the strong H^1 convergence of $\mathcal{I}_h(\cdot)$ and the weak H^1 convergence of S_n, respectively, like in Step 2.

Also,

$$
\begin{aligned}
T_2 &= \left(\left| \nabla \mathbf{U}_n \right|^2 S_n, \mathcal{I}_h(\varphi) \right) + \left(\left| \nabla \mathbf{U}_n \right|^2 S_n, \varphi - \mathcal{I}_h(\varphi) \right) \\
&\quad + \left(\left(\left| \nabla \mathbf{u} \right|^2 - \left| \nabla \mathbf{U}_n \right|^2 \right) S_n, \varphi \right) + \left(\left| \nabla \mathbf{u} \right|^2 \left(s - S_n \right), \varphi \right) \\
&=: T_{21}^n + T_{22}^n + T_{23}^n + T_{24}^n,
\end{aligned}
$$

with $T_{22}^n, T_{23}^n, T_{24}^n \to 0$ by the properties of the Lagrange interpolation, Step 3, and Lemma 5.6, respectively.

Finally

$$
\begin{aligned}
T_3 &= \left(S_n - 1, \mathcal{I}_h(\varphi) \right)_h + \left(S_n - 1, \mathcal{I}_h(\varphi) \right) - \left(S_n - 1, \mathcal{I}_h(\varphi) \right)_h \\
&\quad + \left(S_n - 1, \varphi - \mathcal{I}_h(\varphi) \right) + \left(s - S_n, \varphi \right) \\
&=: T_{31}^n + \ldots + T_{35}^n,
\end{aligned}
$$

with $\left| T_{32}^n + T_{33}^n \right| \leq Ch \left\| \nabla S_n \right\|_{L^2(\Omega)} \left\| \mathcal{I}_h(\varphi) \right\|_{L^2(\Omega)} \to 0$, and $T_{34}^n, T_{35}^n \to 0$ by the strong L^p convergence of $\mathcal{I}_h(\cdot)$ and S_n, respectively.

So, putting all of the above together, we have for $n \in \mathbb{N}$ and $h > 0$ fixed,

$$2\alpha\varepsilon\left(\nabla s, \nabla\varphi\right) + \gamma\left(|\nabla\mathbf{u}|^2 s, \varphi\right) + \frac{\alpha}{2\varepsilon}\left(s - 1, \varphi\right) =: 2\alpha\varepsilon T_{13}^n + \gamma T_{21}^n + \frac{\alpha}{2\varepsilon}T_{31}^n + T^n,$$

where $2\alpha\varepsilon T_{13}^n + \gamma T_{21}^n + \frac{\alpha}{2\varepsilon}T_{31}^n = 0$ by construction. Now, letting $n \to +\infty$ and $h \to 0$, we get $T^n \to 0$, as shown above.

By a density argument, s solves equation (5.3) for $\varphi \in H^1(\Omega) \cap L^\infty(\Omega)$. And since replacing s pointwise by $0 \vee s \wedge 1$ would only decrease every term of this energy, $0 \leq s \leq 1$ follows.

$\square$

Remark 5.7. *For $d \leq 2$, one can also get $\nabla S_n \to \nabla s$ strongly in $L^2(\Omega; \mathbb{R}^m)$, with an argument similar to Step 3, using the equations for S_n and s and a test function $R_h(s) - S_n$. It breaks down for $d \geq 3$ because of the lack of L^∞-stability of the Ritz projection.*

6. Computational Studies

To implement Algorithm 5.2, we use a simple fixed-point strategy (with 3 iterations) for the Ginzburg-Landau term.

To process real images, we suggest to amend Ambrosio and Tortorelli's energy to $AT_\varepsilon(\mathbf{u}, v, s)$: $H^1\left(\Omega, \mathbb{S}^{m-1}\right) \times H^1(\Omega) \times H^1(\Omega) \to [0, +\infty]$

(6.1)
$$
\begin{aligned}
AT_\varepsilon(\mathbf{u}, v, s) \quad := \quad & \frac{\gamma}{2}\int_\Omega \left(s^2 + k_\varepsilon\right)|\nabla\mathbf{u}|^2\mathrm{d}\mathbf{x} + \frac{\lambda}{2}\int_\Omega |\mathbf{u} - \mathbf{g}|^2\mathrm{d}\mathbf{x} \\
& + \frac{\gamma_1}{2}\int_\Omega \left(s^2 + k_\varepsilon\right)|\nabla v|^2\mathrm{d}\mathbf{x} + \frac{\lambda_1}{2}\int_\Omega |v - b|^2\mathrm{d}\mathbf{x} \\
& + \alpha\int_\Omega \varepsilon|\nabla s|^2 + \frac{1}{4\varepsilon}(1 - s)^2\mathrm{d}\mathbf{x},
\end{aligned}
$$

with $\gamma, \gamma_1, \alpha, \lambda, \lambda_1$ positive constants and $b, v \in L^\infty(\Omega) \cap H^1(\Omega)$ the brightness component of the original and the processed image, respectively (normalised to lie in $[0, 1]$). So, we add a smoothing and a fidelity term for the brightness component in the second line of (6.1). The idea here is that the smoothing term for the chromaticity component forces $|s|$ to be small whenever $|\nabla\mathbf{u}|$ is large, while the smoothing term for the brightness component does the same whenever $|\nabla v|$ is large. So we expect $\{s \approx 0\}$ to approximate the union of the essential jump sets of the chromaticity and the brightness component.

This necessitates the adaptation of the optimisation problem for s as well as the solution of a third optimisation problem, which we place between the two existing ones.

If we process an image with more noise in the chromaticity as in the brightness, as is usually the case with images from digital cameras, we can now choose to give more weight to the information of the brightness component, and the chromaticity component will profit from the better information of the brightness component through the joint edge set, as illustrated in Example 5.

6.1. **Academic Images, Splitting & Projection.** All arrows below are scaled in length to fit the plots. What we call h below is the length of the two shorter sides of the rectangular triangles in our triangulations; i.e., it is shorter than the actual diameter of the triangles (by a factor of $\sqrt{2}$).

Example 1. *Let $\Omega := (0, 1)^2$ and $\mathbf{G}$ as in the left plot in Figure 2. The right picture shows a section along $x = 0.5$, where the z-values of the two regions are the closest. We use a triangulation consisting of 2^{2*8} halved squares (along the direction $(1, 1)$); i.e., 131072 triangles, with 66049 nodes, and $h = 2^{-8} \approx 4 * 10^{-3}$. The initial values for $\mathbf{U}$ and S are $\mathbf{U}_0 \equiv \mathbf{G}$ and $S_0 \equiv 0.5$, respectively. We choose $\gamma = 1.2$, $\alpha = 0.5$, $\lambda = 2 * 10^3$, $\varepsilon = 6 * 10^{-4}$, and $k_\varepsilon = 10^{-6}$ (parameters chosen by experiment).*

Figure 2 shows the initial values, Figure 3 the result after 10 iterations of our proposed algorithm. Figure 4 shows the detected edge set and Figure 5 the Ambrosio-Tortorelli energy over time.

The next example numerically studies blowup behaviour for the $W^{1,\infty}$-norm of iterates $\{\mathbf{U}_n, S_n\}$ in the absence of a fidelity term; i.e., $\lambda = 0$. This is motivated by blowup results for harmonic maps (to the sphere), see e.g. [46, 47, 48, 49, 37, 6]. In particular, it is known that for $d = 2$, singularities only appear for large initial energy. And any harmonic map (for general d) is smooth outside a set whose $(d - 2)$-dimensional Hausdorff measure is zero, see [45, 46, 38, 29, 9, 41, 40].

Example 2. *Let Ω be as above. We first use a triangulation consisting of 2^{2*r}, $r = 8$ halved squares as above, and later use coarser ones ($r \in \{5, \ldots, 8\}$) for comparison. Let $\gamma = 1 = \alpha$, $\lambda = 0$, $\varepsilon = h/6$, and $k_\varepsilon = 10^{-6}$. We use two sets of initial data for $\mathbf{U}$ and S, which are shown in Figures 6 and 9 (leftmost column). In both cases, $\mathbf{U}_0$ is constantly $(0, 0, 1)$ in the periphery of the image, $(0, 0, -1)$ at the centre,*
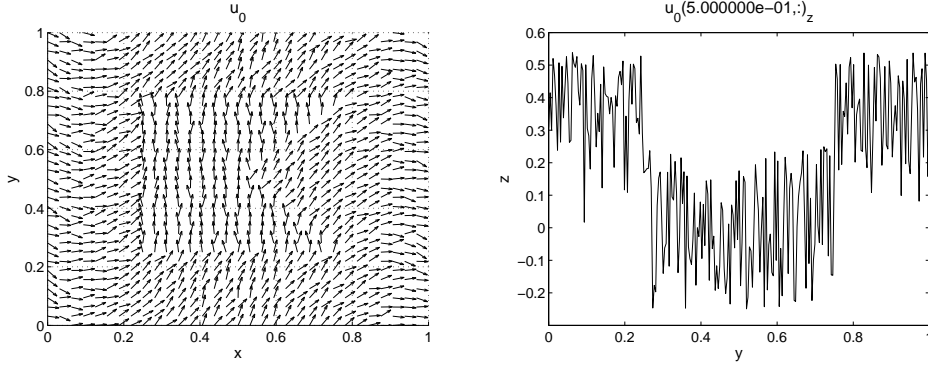
FIGURE 2. Example 1: Original image (left) and z-values of a vertical section through it ($x = 0.5$, right).

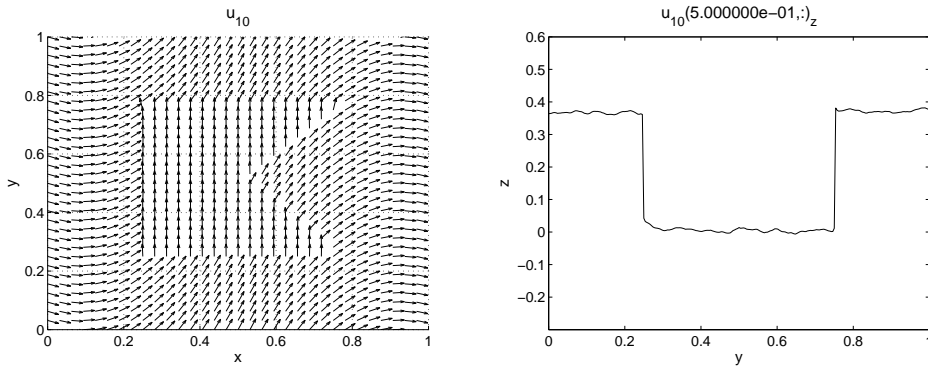FIGURE 3. Example 1: Image and section after 10 iterations.

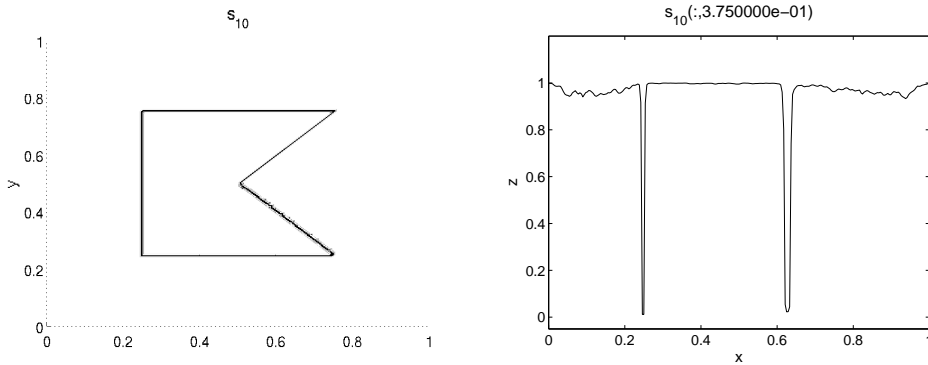

FIGURE 4. Example 1: Edge set (left) and horizontal section through it ($y = 0.375$, right) after 10 iterations.

and varying continuously inside a circle around the centre. In the first case, we choose $S = 0$ at the centre, $S = 1$ in the periphery, and smoothly varying in between; in the second case, we choose $S = 1$ at the centre, $S = 0$ in the periphery, and smoothly varying in between.

Figure 6 shows iterates $n \in \{0, 3, 5\}$ for $r = 8$ (crops in the case of $\mathbf{U}_n$), Figure 7 shows the total energy for $r \in \{5, \ldots, 8\}$, while Figure 8 shows the $W^{1,\infty}$-norms of $\mathbf{U}_n$ and S_n for $r \in \{5, \ldots, 8\}$, which both show blowup behaviour. This time it is $\mathbf{U}_n$ which appears one step ahead of S_n with respect to blowup behaviour. Depending somewhat on r, the system matrices become close to singular after 6–7 iterations, so after this point, the results can no longer be expected to be reliable. The arrow at the centre of $\mathbf{U}$ at this point still points down, while the rest of $\mathbf{U}$ points up. The variable S, on the other hand, becomes 1 everywhere, except for the centre, where it stays 0. After breakdown, the arrows move erratically, but perfectly synchronised with one another.

16
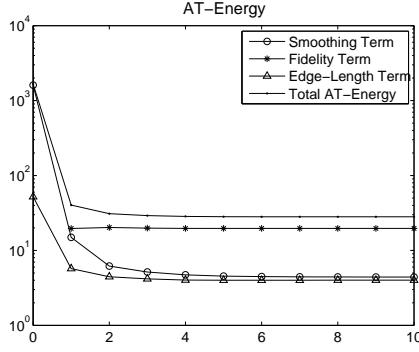
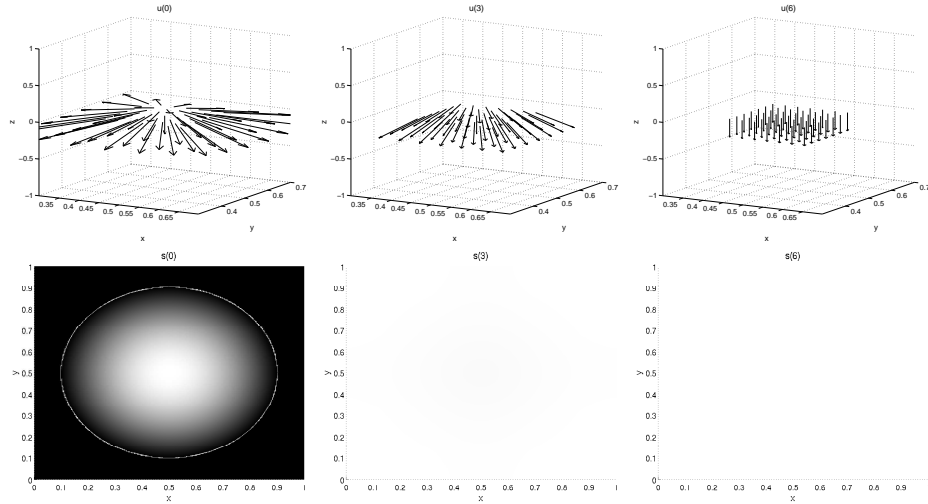FIGURE 5. Example 1: Ambrosio-Tortorelli Energy (10 iterations, logarithmic plot).
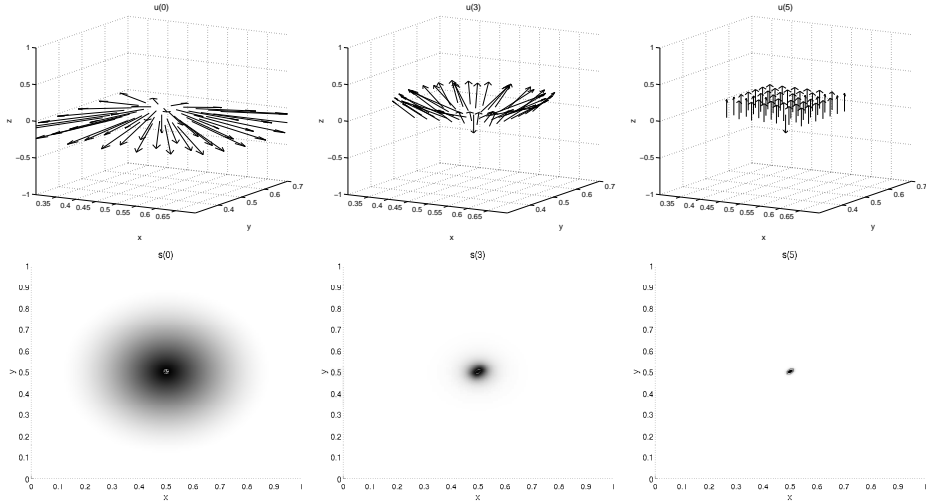
FIGURE 6. Example 2: Detail of $\mathbf{U}_n$ (top) and full image of S_n (bottom) for $n \in \{0, 3, 5\}$.
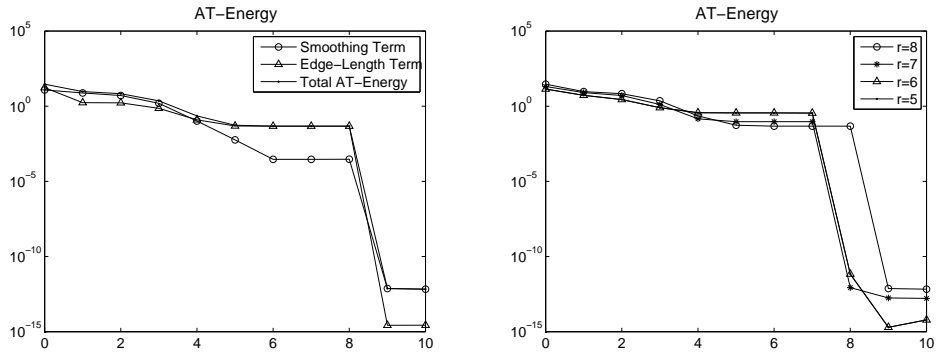
FIGURE 7. Example 2: Ambrosio-Tortorelli energy, 10 steps, for $r = 8$ (left) and $r \in \{5, \ldots, 8\}$ (right), y-logarithmic plots.

The next example uses the same setting and the same initial data for $\mathbf{U}$, but avoids blowup behaviour through a different choice of initial data for S.

Example 3. *Except for the initial data for S we use exactly the same setting as in Example 2. This time, we choose $S = 1$ at the centre, $S = 0$ in the periphery, and smoothly varying in between.*

Figure 9 shows iterates $n \in \{0, 3, 6\}$ for $r = 8$ (crops in the case of $\mathbf{U}_n$), Figure 10 shows the total energy for $r \in \{5, \ldots, 8\}$, while Figure 11 shows the $W^{1,\infty}$-norms of $\mathbf{U}_n$ and S_n for $r \in \{5, \ldots, 8\}$, which this time stay finite. The arrows of $\mathbf{U}$ all point down at the end, while S is 1 everywhere. After

17
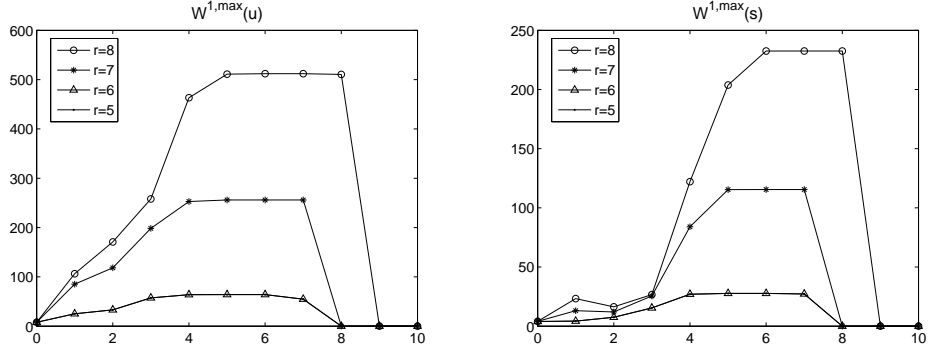
FIGURE 8. Example 2: $W^{1,\infty}$-norm of $\mathbf{U}$ and S for $r \in \{5, \ldots, 8\}$.

FIGURE 9. Example 3: Detail of $\mathbf{U}_n$ (top) and S_n (bottom) for $n \in \{0, 3, 6\}$.
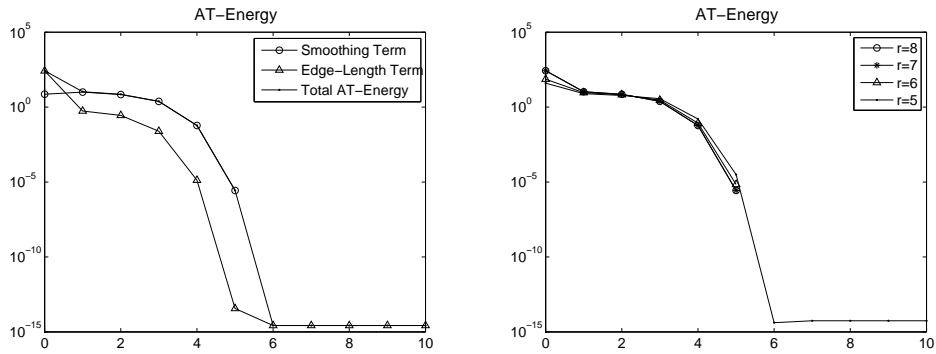
FIGURE 10. Example 3: Ambrosio-Tortorelli energy, 10 steps, for $r = 8$ (left) and $r \in \{5, \ldots, 8\}$ (right), y-logarithmic plots.

6 iterations, the system matrices again become close to singular; in this case, however, iterates do not change dramatically after this point, if at all.

6.2. **Academic Images, Penalisation & Splitting.** The next example studies the same setting as Example 1, this time with Algorithm 5.2; i.e., the sphere constraint is enforced by penalisation instead of projection. Again, all arrows are scaled in length to fit the plots.

Example 4. *The setting is as in Example 1. Parameters are $\gamma = 1.2$, $\alpha = 0.5$, $\lambda = 2 * 10^3$, $\varepsilon = 10^{-3}$, $k_\varepsilon = 10^{-6}$, and $\delta_\varepsilon = 0.1$ (chosen by experiment).*
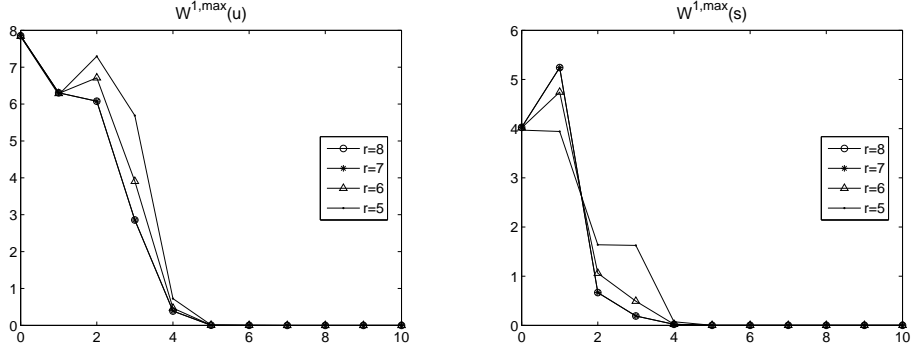
FIGURE 11. Example 3: $W^{1,\infty}$-norm of $\mathbf{U}$ and S for $r \in \{5, \ldots, 8\}$.
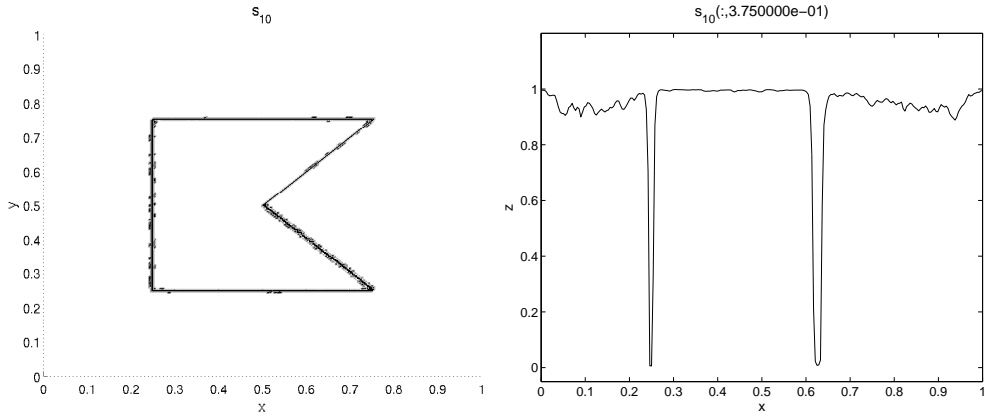
FIGURE 12. Example 4: Edge set (left) and horizontal section through it ($y = 0.375$, right) after 10 iterations.
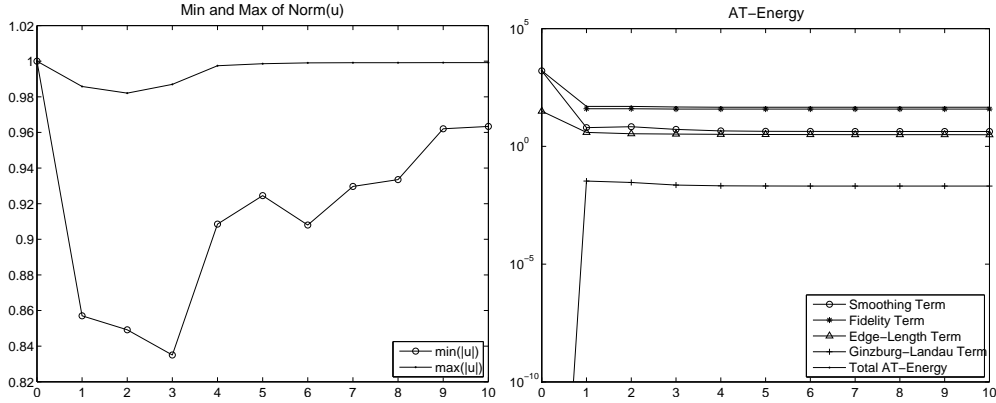
FIGURE 13. Example 4: min and max of $|\mathbf{U}|$ (left), and Ambrosio-Tortorelli Energy (right) for 10 iterations.

The result $\mathbf{U}$ after 10 iterations looks just like in Example 1 (Figure 3), so we omit the corresponding figures. The detected edge set after 10 iterations, however, is less exact, as shown in Figure 12. Figure 13 shows the global minimum and maximum of $|\mathbf{U}|$ and the Ambrosio-Tortorelli energy over time.

For δ_ε between about $5 * 10^{-3}$ and at least 10^2, the results are qualitatively very similar to the ones in Example 1, but the detected edge set is less exact, and $|\mathbf{U}|$ can be quite a bit shorter than 1. For δ_ε smaller than $5 * 10^{-3}$ (which would be advantageous for the accuracy of $|\mathbf{U}|$), the results break down, which is in accordance with our theoretical results.

6.3. **Real Image, Splitting & Projection.**

Example 5. *We try our algorithm on a small photograph (399 × 299 pixels), as shown in Figure 14. We choose $\Omega := (0, 399/299) \times (0, 1)$, whence $h = 1/298 \approx 3 * 10^{-3}$, the pixels are used as nodes, each square of 4 pixels giving rise to two triangles. We further choose $S_0 \equiv 1$ and add two different kinds of noise to the image:*

(1) *RGB noise: $R = R_0 + 0.3 * \mathrm{randn}$, and G and B analogously, where randn are pseudo-random values drawn from the standard normal distribution. After this operation, we crop R, G, and B to lie in $[0, 1]$ (where R_0, G_0, B_0 were scaled to lie). This is shown in Figure 14.*

(2) *CB noise, mainly in the chromaticity component: $\mathbf{C} = \mathbf{C}_0 + 0.5 * \mathrm{randn} * \mathbf{C}_0 \times [1, 1, 1] \in \mathbb{S}^2$, and $B = B_0 + 0.01 * \mathrm{randn}$. After this operation, $\mathbf{C}$ is projected onto the sphere, and B is cropped to lie in $[0, 1]$. This is shown in Figure 18.*

Our CB algorithm was in both cases compared to a channelwise RGB computation for the same image, with all channels sharing the same edge set. Parameters were chosen as follows (by experiment):

(1) *RGB computation: $\alpha = 0.3$, $\beta = 10^{-2}$, $\gamma = 10^3$, $\varepsilon = 10^{-4}$, and $k_\varepsilon = 10^{-7}$.*
    CB computation: $\alpha = \alpha_1 = 0.5$, $\beta = 8 * 10^{-3}$, $\gamma = \gamma_1 = 10^3$, $\varepsilon = 10^{-4}$, and $k_\varepsilon = 10^{-7}$.

(2) *RGB computation: $\alpha = 0.5$, $\beta = 5 * 10^{-3}$, $\gamma = 50$, $\varepsilon = 10^{-4}$, and $k_\varepsilon = 10^{-7}$.*
    CB computation: $\alpha = \alpha_1 = 0.3$, $\beta = 5 * 10^{-2}$, $\gamma = 10^2$, $\gamma_1 = 5 * 10^5$, $\varepsilon = 10^{-4}$, and $k_\varepsilon = 10^{-7}$.

FIGURE 14. Example 5.1: Original image (left) and image with RGB noise (right).

FIGURE 15. Example 5.1: Image after 10 iterations, RGB (left) and CB (right).

First, let us look at the computations with RGB noise: Figure 14 shows the noisy initial image, and Figure 15 the results after 10 iterations. Figure 16 shows the detected edge sets, and Figure 17 the expanded Ambrosio-Tortorelli energy over time. The energy terms labelled "...C" belong to the chromaticity component, those labelled "...B" to the brightness. The channelwise RGB algorithm has the advantage here.

Next, let us look at the image with CB noise: Figure 18 shows the noisy initial image, and Figure 19 the results after 10 iterations. Figure 20 shows the detected edge sets, and Figure 21 the expanded Ambrosio-Tortorelli energy over time. The CB algorithm has a very clear advantage here.
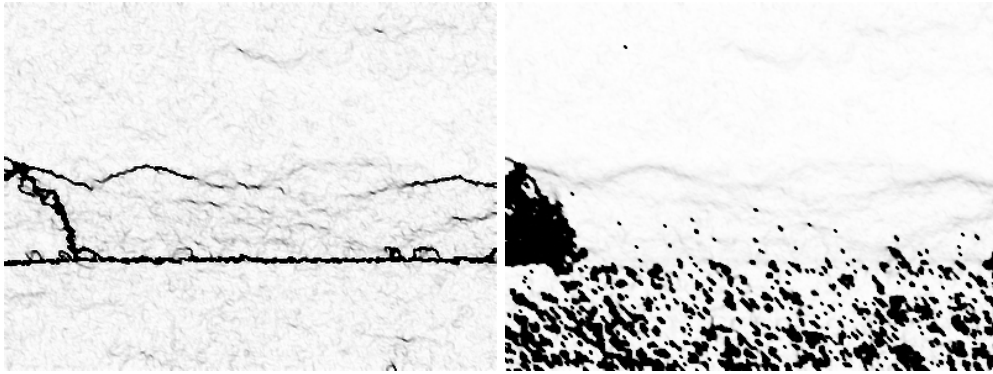
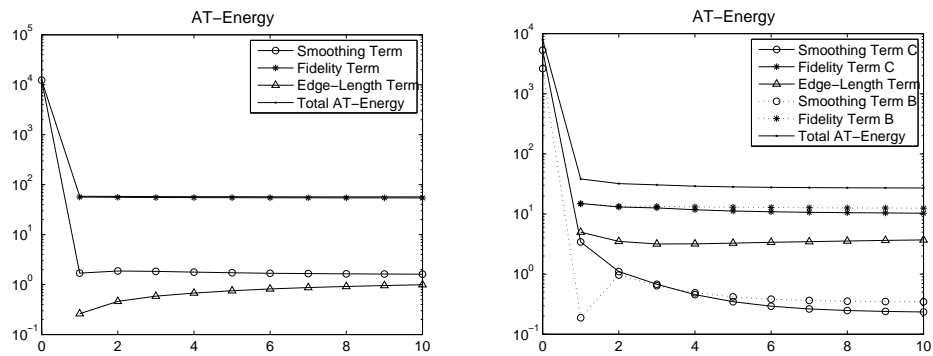FIGURE 16. Example 5.1: Edge set, RGB (left) and CB (right).

FIGURE 17. Example 5.1: Expanded Ambrosio-Tortorelli Energy (10 iterations, y-logarithmic plots), RGB (left) and CB (right).
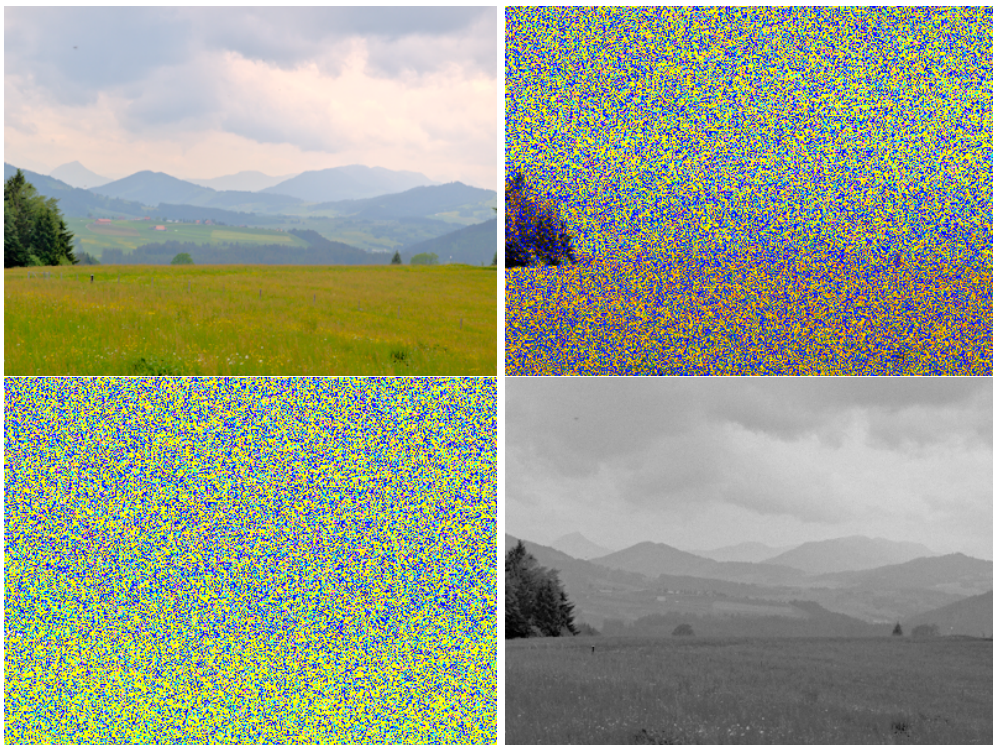

FIGURE 18. Example 5.2: Original image and image with CB noise (top), as well as noisy chromaticity (bottom left) and brightness (bottom right) components.

FIGURE 19. Example 5.2: Image after 10 iterations, RGB (left) and CB (right).
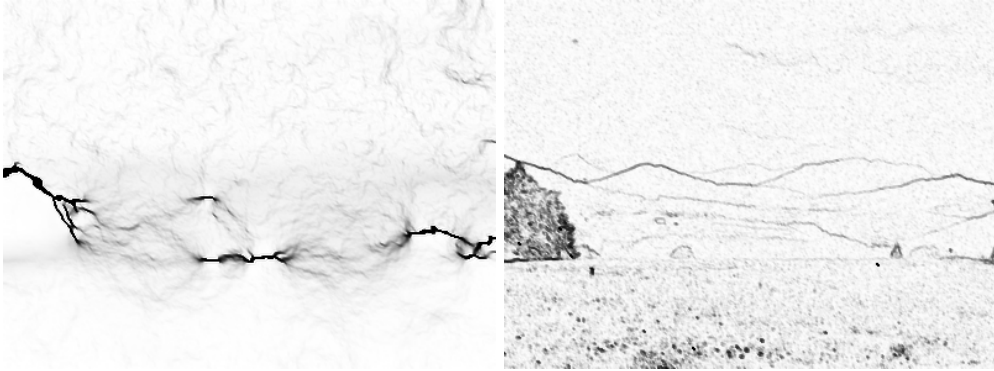

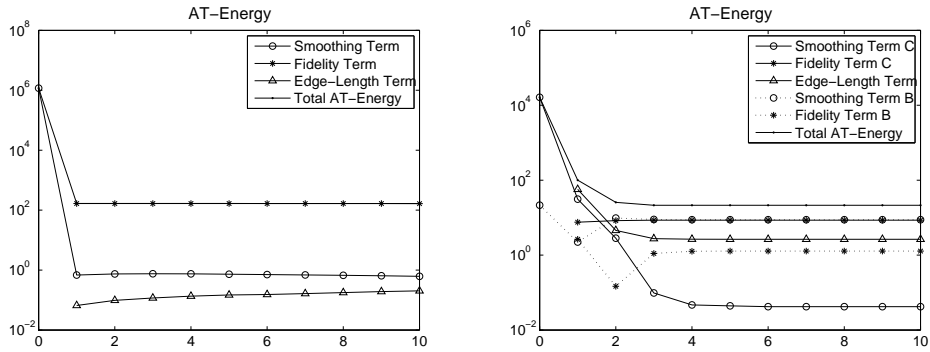FIGURE 20. Example 5.2: Edge set, RGB (left) and CB (right).

FIGURE 21. Example 5.2: Expanded Ambrosio-Tortorelli Energy (10 iterations, y-logarithmic plots), RGB (left) and CB (right).

ACKNOWLEDGEMENTS

REFERENCES

[1] F. Alouges. A new algorithm for computing liquid crystal stable configurations: the harmonic mapping case. *SIAM J. Numer. Anal.*, 34(5):1708–1726, 1997.

[2] L. Ambrosio, N. Fusco, and D. Pallara. *Functions of bounded variation and free discontinuity problems*. Oxford Mathematical Monographs. The Clarendon Press Oxford University Press, New York, 2000.

[3] L. Ambrosio and V. M. Tortorelli. Approximation of functionals depending on jumps by elliptic functionals via Γ-convergence. *Comm. Pure Appl. Math.*, 43(8):999–1036, 1990.

[4] L. Ambrosio and V. M. Tortorelli. On the approximation of free discontinuity problems. *Boll. Un. Mat. Ital. B (7)*, 6(1):105–123, 1992.

[5] S. Bartels. Stability and convergence of finite-element approximation schemes for harmonic maps. *SIAM J. Numer. Anal.*, 43(1):220–238 (electronic), 2005.

[6] S. Bartels and A. Prohl. Constraint preserving implicit finite element discretization of harmonic map flow into spheres. *Math. Comp.*, 76(260):1847–1859 (electronic), 2007.

[7] S. Bartels and A. Prohl. Stable discretization of scalar and constrained vectorial Perona-Malik equation. *Interfaces Free Bound.*, 9(4):431–453, 2007.

[8] G. Bellettini and A. Coscia. Discrete approximation of a free discontinuity problem. *Numer. Funct. Anal. Optim.*, 15(3-4):201–224, 1994.

[9] F. Bethuel. On the singular set of stationary harmonic maps. *Manuscripta Math.*, 78(4):417–443, 1993.

[10] B. Bourdin. Image segmentation with a finite element method. *M2AN Math. Model. Numer. Anal.*, 33(2):229–244, 1999.

[11] A. Braides. *Approximation of free-discontinuity problems*, volume 1694 of *Lecture Notes in Mathematics*. Springer-Verlag, Berlin, 1998.

[12] A. Braides. *Γ-convergence for beginners*, volume 22 of *Oxford Lecture Series in Mathematics and its Applications*. Oxford University Press, Oxford, 2002.

[13] A. Braides and G. Dal Maso. Non-local approximation of the Mumford-Shah functional. *Calc. Var. Partial Differential Equations*, 5(4):293–322, 1997.

[14] S. C. Brenner and L. R. Scott. *The mathematical theory of finite element methods*, volume 15 of *Texts in Applied Mathematics*. Springer-Verlag, New York, second edition, 2002.

[15] S. Burke, C. Ortner, and E. Süli. An adaptive finite element approximation of a variational model of brittle fracture. *OxMOS Preprint No. 16*, 2008.

[16] M. C. Calderer, D. Golovaty, F.-H. Lin, and C. Liu. Time evolution of nematic liquid crystals with variable degree of orientation. *SIAM J. Math. Anal.*, 33(5):1033–1047 (electronic), 2002.

[17] M. Carriero and A. Leaci. S^k-valued maps minimizing the L^p-norm of the gradient with free discontinuities. *Ann. Scuola Norm. Sup. Pisa Cl. Sci. (4)*, 18(3):321–352, 1991.

[18] A. Chambolle. Inverse problems in image processing and image segmentation: some mathematical and numerical aspects. In C. E. Chidume, editor, *Mathematical Problems in Image Processing*. ICTP, December 2000. ICTP Lecture Notes Series, Vol 2, URL: http://publications.ictp.it/lns/vol2.html.

[19] T. F. Chan, S. H. Kang, and J. Shen. Total variation denoising and enhancement of color images based on the CB and HSV color models. *J. Visual Comm. Image Rep.*, 12(4):422–435, 2001.

[20] P. Clément. Approximation by finite element functions using local regularization. *Rev. Française Automat. Informat. Recherche Opérationnelle Sér. RAIRO Analyse Numérique*, 9(R-2):77–84, 1975.

[21] R. Cohen, S. Y. Lin, and M. Luskin. Relaxation and gradient methods for molecular orientation in liquid crystals. *Comput. Phys. Comm.*, 53(1-3):455–465, 1989. Practical iterative methods for large scale computations (Minneapolis, MN, 1988).

[22] G. Cortesani. A finite element approximation of an image segmentation problem. *Math. Models Methods Appl. Sci.*, 9(2):243–259, 1999.

[23] G. Dal Maso. *An introduction to Γ-convergence*. Progress in Nonlinear Differential Equations and their Applications, 8. Birkhäuser Boston Inc., Boston, MA, 1993.

[24] E. De Giorgi. Free discontinuity problems in calculus of variations. In *Frontiers in pure and applied mathematics*, pages 55–62. North-Holland, Amsterdam, 1991.

[25] E. De Giorgi. Variational free-discontinuity problems. In *International Conference in Memory of Vito Volterra (Italian) (Rome, 1990)*, volume 92 of *Atti Convegni Lincei*, pages 133–150. Accad. Naz. Lincei, Rome, 1992.

[26] E. De Giorgi and L. Ambrosio. New functionals in the calculus of variations. *Atti Accad. Naz. Lincei Rend. Cl. Sci. Fis. Mat. Natur. (8)*, 82(2):199–210 (1989), 1988.

[27] E. De Giorgi, M. Carriero, and A. Leaci. Existence theorem for a minimum problem with free discontinuity set. *Arch. Rational Mech. Anal.*, 108(3):195–218, 1989.

[28] F. Dibos and E. Séré. An approximation result for the minimizers of the Mumford-Shah functional. *Boll. Un. Mat. Ital. A (7)*, 11(1):149–162, 1997.

[29] L. C. Evans. Partial regularity for stationary harmonic maps into spheres. *Arch. Rational Mech. Anal.*, 116(2):101–113, 1991.

[30] L. C. Evans and R. F. Gariepy. *Measure theory and fine properties of functions*. Studies in Advanced Mathematics. CRC Press, Boca Raton, FL, 1992.

[31] H. Federer. *Geometric measure theory*. Die Grundlehren der mathematischen Wissenschaften, Band 153. Springer-Verlag New York Inc., New York, 1969.

[32] M. Focardi. On the variational approximation of free-discontinuity problems in the vectorial case. *Math. Models Methods Appl. Sci.*, 11(4):663–684, 2001.

[33] M. Focardi. *Variational Approximation of Vectorial Free Discontinuity Problems: the Discrete and Continuous Case*. PhD thesis, Scuola Normale Superiore di Pisa, 2002. URL: http://cvgmt.sns.it/papers/foc01/.

[34] D. Gilbarg and N. S. Trudinger. *Elliptic partial differential equations of second order*, volume 224 of *Grundlehren der Mathematischen Wissenschaften [Fundamental Principles of Mathematical Sciences]*. Springer-Verlag, Berlin, second edition, 1983.

[35] E. Giusti. *Minimal surfaces and functions of bounded variation*, volume 80 of *Monographs in Mathematics*. Birkhäuser Verlag, Basel, 1984.

[36] J. Haehnle. *Numerical Analysis of the Mumford-Shah and Mumford-Shah-Euler Functionals for Sphere-Valued Functions, and applications to Numerical Image Processing.* PhD thesis, Tübingen, 2010.

[37] R. M. Hardt. Singularities of harmonic maps. *Bull. Amer. Math. Soc. (N.S.)*, 34(1):15–34, 1997.

[38] F. Hélein. Régularité des applications faiblement harmoniques entre une surface et une variété riemannienne. *C. R. Acad. Sci. Paris Sér. I Math.*, 312(8):591–596, 1991.

[39] F.-H. Lin. Nonlinear theory of defects in nematic liquid crystals; phase transition and flow phenomena. *Comm. Pure Appl. Math.*, 42(6):789–814, 1989.

[40] F.-H. Lin. Gradient estimates and blow-up analysis for stationary harmonic maps. *Ann. of Math. (2)*, 149(3):785–829, 1999.

[41] F. H. Lin and C. Y. Wang. Stable stationary harmonic maps to spheres. *Acta Math. Sin. (Engl. Ser.)*, 22(2):319–330, 2006.

[42] S. Y. Lin and M. Luskin. Relaxation methods for liquid crystal problems. *SIAM J. Numer. Anal.*, 26(6):1310–1324, 1989.

[43] D. Mumford and J. Shah. Optimal approximations by piecewise smooth functions and associated variational problems. *Comm. Pure Appl. Math.*, 42(5):577–685, 1989.

[44] S. J. Osher and L. A. Vese. Numerical methods for p-harmonic flows and applications to image processing. *SIAM J. Numer. Anal.*, 40(6):2085–2104 (electronic) (2003), 2002.

[45] R. Schoen and K. Uhlenbeck. A regularity theory for harmonic maps. *J. Differential Geom.*, 17(2):307–335, 1982.

[46] R. Schoen and K. Uhlenbeck. Regularity of minimizing harmonic maps into the sphere. *Invent. Math.*, 78(1):89–100, 1984.

[47] M. Struwe. On the evolution of harmonic mappings of Riemannian surfaces. *Comment. Math. Helv.*, 60(4):558–581, 1985.

[48] M. Struwe. Geometric evolution problems. In *Nonlinear partial differential equations in differential geometry (Park City, UT, 1992)*, volume 2 of *IAS/Park City Math. Ser.*, pages 257–339. Amer. Math. Soc., Providence, RI, 1996.

[49] M. Struwe. *Variational methods*, volume 34 of *Ergebnisse der Mathematik und ihrer Grenzgebiete. 3. Folge. A Series of Modern Surveys in Mathematics [Results in Mathematics and Related Areas. 3rd Series. A Series of Modern Surveys in Mathematics]*. Springer-Verlag, Berlin, third edition, 2000. Applications to nonlinear partial differential equations and Hamiltonian systems.

[50] B. Tang, G. R. Sapiro, and V. Caselles. Color image enhancement via chromaticity diffusion. *IEEE Transactions on Image Processing*, 10(5):701–707, May 2001.

[51] E. G. Virga. *Variational theories for liquid crystals*, volume 8 of *Applied Mathematics and Mathematical Computation*. Chapman & Hall, London, 1994.

Mathematisches Institut, Universität Tübingen, Auf der Morgenstelle 10, D-72076 Tübingen, Germany

E-mail address: haehnle@na.uni-tuebingen.de